COMPUTATIONAL MODELING: THE EFFECTS OF MOTION ON TOTAL KNEE REPLACEMENTS

By

MATTHEW A. HAMILTON

A THESIS PRESENTED TO THE GRADUATE SCHOOL OF THE UNIVERSITY OF FLORIDA IN PARTIAL FULFILLMENT OF THE REQUIREMENTS FOR THE DEGREE OF MASTER OF SCIENCE

UNIVERSITY OF FLORIDA

2003

ACKNOWLEDGMENTS

I wish to thank Dr. Greg Sawyer for his guidance and support on not only the present project, but past and future ones as well. I also appreciate the help of Dr. Ziegert and Dr. Arakere throughout my time at the University of Florida and for agreeing to review this work. Special thanks go to all the members of the Tribology Lab (Aaron Ison, Jason Action, Dan and Pam Dickrell, Darren McGuire, Brian Micklos and Dave Burris) for help provided in their various fields of expertise.

I would like to thank my parents for their support through all my years in school.

I would like to thank my wife, Melissa. Her encouragement throughout this endeavor has helped me tremendously. Without her I could not have achieved this goal.

TABLE OF CONTENTS

LIST OF TABLES

LIST OF FIGURES

Figure page

Abstract of Thesis Presented to the Graduate School
of the University of Florida in Partial Fulfillment of the
Requirements for the Degree of Master of Science

COMPUTATIONAL MODELING: THE EFFECTS OF MOTION ON TOTAL KNEE REPLACEMENTS

By

Matthew A. Hamilton

May 2003

Chair: W. Gregory Sawyer
Department: Mechanical and Aerospace Engineering

Total knee replacements have evolved significantly in the past half-century. A major development, the use of Ultra-High Molecular-Weight Polyethylene (UHMWPE), has increased functional life to more than a decade. Although the occurrence of failures in current TKRs is low, wear and its results still plague the total joint replacement. Wearing of the UHMWPE tibial bearing changes its geometry allowing the femoral component to move in ways not intended by manufacturers. This loosening results in instability and poor functionality in the joint. When the joint no longer functions as intended, the recourse is revision surgery. Due to the loss of bone surrounding the joint from osteolysis and the original implant surgery, doctors are left with little to work with when revising a TKR. This results in success rates of revision surgery is below 70% causing major concern to patients at higher risk for component failure.

The focus of current research is to increase the life of the components by developing a tool capable of aiding researchers in the design-stage of TKR production. By allowing designers to identify possible design flaws prior to prototyping, the testing of new designs would be expedited. A tool of this nature would help reduce the workload

for knee simulator testing. Testing in a knee simulator is not only time consuming (each test could take up to four months), but it is also expensive (average cost $40,000). Thus, new ideas could get from the drawing board to the doctor's office more quickly and at a lower cost.

The purpose of this project was to develop a tool, which could use fluoroscopic data from a patient performing a set of exercises, to predict the effect of these motions on a TKR over a finite period of time. The motions experienced by the surface of the bearing were evaluated to establish a method of categorizing motions based on their ability to damage the surface. Wear and creep damage predictions were made based on a variety of motion inputs. These damage predictions, made using the software, were compared to actual data from a retrieved tibial bearing component. Finally, the thermal effects created by motions in the knee were evaluated. Although it is not likely that thermal effects created by everyday activity could be a factor, those experienced in knee simulators may be sufficient to affect results.

The tool developed accurately predicted wear geography, which is a first step toward predicting total damage. Also tools for quantifying multidirectional motion and temperature rise due to frictional heating were developed. The crossing motion results give an indication of the severity of crossing in a particular motion. Thermal results from frictional heating were from 10 to $15^{o}C$.

CHAPTER 1
INTRODUCTION

The evolution of the Total Knee Replacement (TKR) began in the early 1940s. The first generation of TKR consisted of a hinge joint, which connected the femur to the tibia. Although the mechanism provided short-term pain relief, its motion was limited and had severe problems with loosening and infection. As a result, the design was abandoned after a few years. The second-generation prosthesis, the McKeever developed in1957 and the MacIntosh developed in 1958, were simply metal plates separating the tibia and femur. The theory behind the plate was to prevent rubbing of irregular surfaces. These devices had mild success, but were unpredictable and did not relieve symptoms in many patients. The next generation of design came from Massachusetts General Hospital. It was a mold type arthroplasty designed to replace the femoral half of the knee joint, but like its predecessors it was unpredictable and failed after short periods of use.

A new era of knee replacement came about in the 1960s, when Frank Gunston, an orthopedist from Sir John Charnley's Hip Center, developed a metal on plastic knee replacement. The prosthesis was cemented directly to the bone, and was the first metal and plastic knee (introduced in 1968). In 1972, Dr. John Insall developed a prototype for the current total knee replacement. To replace all the surfaces in the knee the prosthesis had three components – the femur, tibia and patella. The components were attached to the bones using bone cement. Since the development of the metal and plastic replacement researchers have been testing new designs and materials to increase the versatility and durability of the arthroplasty. A major development was the polymer

Ultra-High Molecular-Weight Polyethylene (UHMWPE). The polymer has been the choice for bearing material for the past 30 years, replacing the original bearing choice Polytetrafluoroethylene (Teflon)(Oonishi, Ishimaru, and Kato, 1996). UHMWPE and Teflon are both biocompatible, however, UHMWPE has a much higher wear resistance. This plastic has increased the useful-life of TKRs. Current replacements have success rates above 90% ten-years after implantation, but the need for increased function and life in the replacements still challenges designers and researchers.

Although the occurrence of failures in current TKRs is 'low,' wear and its results still plague the total joint replacement. Wear is defined as damage to a solid surface, generally involving progressive loss of material, due to relative motion between that surface and a contacting substance or substances. Factors influencing wear are normal load, sliding-distance, friction-coefficient, nominal temperature and environment. The wearing of the components in a TKR has a dual effect on the life of the device. Wearing of the UHMWPE tibial bearing changes its geometry allowing the femoral component to move in ways not intended by manufacturers. Loosening, as a result of wear, causes instability and poor functionality in the joint. Another issue troubling designers of these prostheses is the effect of wear debris generated from the bearing. Although the volume of material worn away by use has decreased with the advent of UHMWPE, the size of the particles itself has become an issue. The average size of a UHMWPE wear particle in knee joint replacements is sub-micron, particles of this size have been labeled the most "biologically active." The body identifies these particles as foreign bodies and triggers defense mechanisms to eliminate them. These defense mechanisms are the source of bone resorption, also called osteolysis, a condition where the bones surrounding the joint

are broken down. This softening of tissue surrounding the TKR causes the components to become unstable, and eventually failure of the TKR. When the joint no longer functions as intended the recourse is revision surgery. Due to the loss of bone surrounding the joint from osteolysis and the original implant surgery, doctors are left with little to work with when revising a TKR. This results in success rates of revision surgery below 70%, causing major concern to patients at higher risk for component failure.

The focus of current research is to increase the life of the components by developing a tool capable of aiding researchers in the design-stage of TKR production. By allowing designers to identify possible design flaws prior to prototyping, the testing of new designs would be expedited. A tool of this nature would help reduce the workload for knee simulator testing. Testing in a knee simulator is not only time consuming (each test could take up to four months), but it is also expensive (average cost $40,000). Thus, new ideas could get from the drawing board to the doctor's office more quickly and at a lower cost.

The purpose of this project was to develop a tool, which could use fluoroscopic data from a patient performing a set of exercises, to predict the effect of these motions on a TKR over a finite period of time. The motions experienced by the surface of the bearing were evaluated to establish a method of categorizing motions based on their ability to damage the surface. Wear and creep damage predictions were made based on a variety of motion inputs. These damage predictions, made using the software, were compared to actual data from a retrieved tibial bearing component. Finally, the thermal effects created by motions in the knee were evaluated. Although it is not likely that

thermal effects created by everyday activity could be a factor, those experienced in knee simulators may be sufficient to affect results.

CHAPTER 2
BACKGROUND AND LITERATURE REVIEW

From the beginning, the durability of TKRs has been a major focus for researchers studying the prostheses. Even the first replacements were studied from the time of implantation to see if the solution was viable for a long-term use. Although the first component designs were not sufficient to sustain activity for long periods of time, they were a valuable first step toward successful replacements. As with any new technology, fledgling attempts are often failures, but the abilities of designers to recognize problems and create new solutions leads to success. The evolution from a simple hinge-joint or a metal plate inserted between two sides of an arthritic joint, to molded metal replacements of the femur with a plastic bearing component cemented directly to the tibia, and finally to replacing the ends of the femur and tibia with anatomically correct metal replacements separated by a molded plastic insert has taken over 50 years. While no standard design has been set, most have the same basic components with subtle variations

The typical TKR consists of three major parts. The femoral condyle, typically made of cobalt-chrome, is connected to the femur using rods protruding from the backside of the component. The tibial plateau is attached to the tibia via a long rod extending down from the bottom of flat metal plate. Finally, the tibial bearing, a molded piece of ultra-high molecular-weight polyethylene, is snapped into the tibial plateau providing a place for the femoral condyle to rest. The way these parts are attached to the bones, and their shapes vary from one design to the next, but these are generally the parts that make up the TKR.

The procedure to insert a total knee replacement involves surgically removing damaged or injured parts of the knee, and replacing them with the components mentioned above. Initially the muscles and ligaments surrounding the knee are separated from the bone, leaving the joint exposed. The ends of the femur and tibia are surgically removed so the pieces of the TKR can be easily attached. Metal rods attached to the backside of the femoral condyle and tibial plateau are forced into the femur and tibia respectively. In some cases the two components are cemented to the bones using bone-cement. The bearing is attached to the tibial plateau, usually it snaps into the surface of the plateau. Some varieties of TKR require the backside of the patella be removed and replaced with a UHMWPE piece as well.

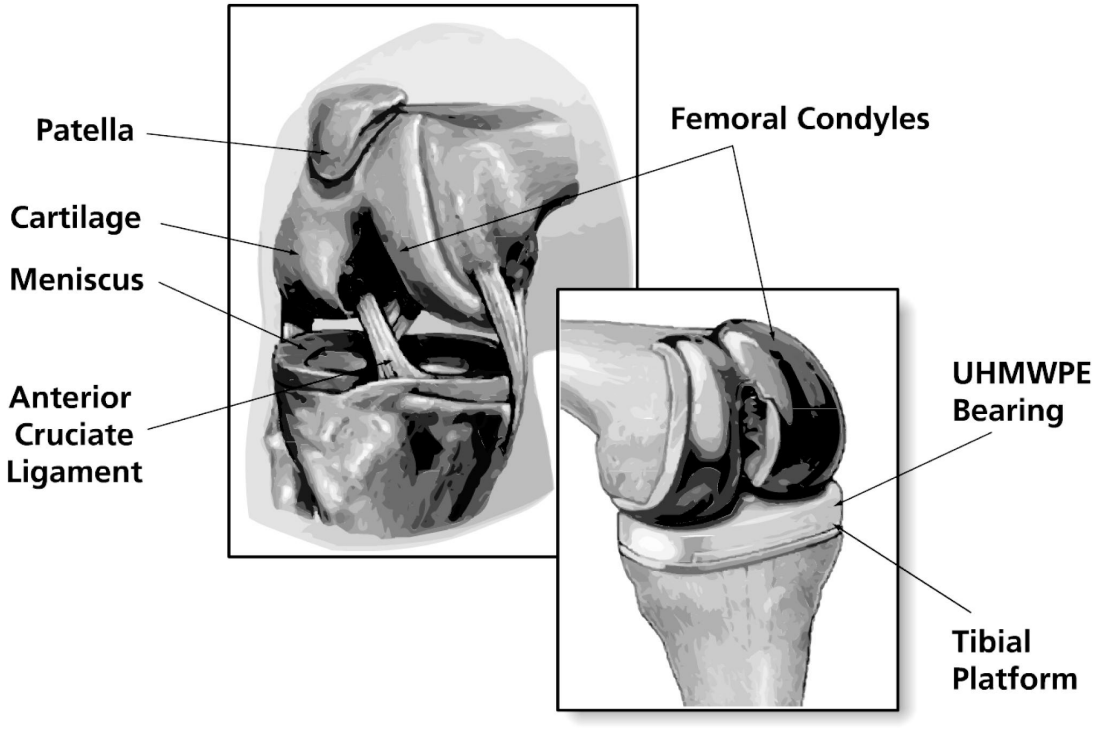

Figure 2-1: Normal knee vs. prosthetic knee.

In an effort to improve the versatility of the TKR, researchers have set out to determine what causes the prostheses to fail. The study of knee replacement survivorship is an active topic demonstrated by Schmalzried and Callaghan (1999) who referenced over 200 articles. Although many designs for knee replacements exist, the results of the studies are very similar. Sextro *et al.* (2001), Pavone *et al.* (2001), Diduch *et al.* (1997), Beuchel *et al.*(2001) and Meding *et al.* (2001) all reported less than 10% failure after a ten-year period. Table 2-1 gives an overview of studies of knee replacement survivorship published over the last 15 years. Figure 2.2 shows a graph of survivorship rates versus years *in vivo*, created from the results of those studies. While the results of these studies indicated that success rates for the implants are 'high,' a variety of observations were made in the studies. Bearing thickness was listed as a variable affecting the success of total knee replacements in multiple studies. Sextro *et al.* (2001) noted that a bearing thickness less than 8 mm significantly increased the chance of failure in the component. Meding *et al.* (2001) also mentioned bearing thickness, although no failures were shown as a result of bearing thickness, the study noted a large increase in knee pain scores for bearings with a thickness of less than 6 mm. Wright *et al.* (1992) found that 11 of the 12 failures found in their study occurred in bearings having a thickness of 6 mm or less. The authors concluded the smaller thickness "increased the stresses on and within the polyethylene."(131) The less-conforming bearing and smaller thickness combined to produce higher stresses, which are emphasized by the "predominance and the severity of the delamination and surface deformation . . . on the retrieved components."(131) Higher stresses are associated with an increase in wear debris which "is a contributory factor . . . to long term complications, especially component loosening."(132) Diduch, Insall, Scott,

Scuderi and Font-Rodriguez (1997) commented on the importance of affixing the components to the bones using cement. The report stated that "cement fixation has also been shown to be an effective barrier against penetration of polyethylene particulate debris."(60) This debris is a major cause of aseptic loosening in the TKR components. Four of the studies (Wright *et al.*, 1992; Sextro *et al.*, 2001; Beuchel *et al.*, 2001; Pavone *et al.*, 2001) noted osteolysis and wear specifically as causes of failure in TKRs studied. Osteolysis or bone resorption is the result of the body trying to eliminate wear particles building up in the tissue and fluid surrounding the knee joint. The failure rates ranged from 2.2% to 4.4% of knees studied failing due to wear or osteolysis. While these percentages seem small, over 266,000 total knee replacements are performed in the United States annually, giving rise to the potential for hundreds of thousands of knees to be affected by wear and its results within the next decade.

Wear is defined as damage to a solid surface, generally involving progressive loss of material, due to relative motion between that surface and a contacting substance or sub-stances. Historically three types have been identified in retrieved total joint replacements: abrasive wear, adhesive wear and fatigue wear. Abrasive wear is a result of plowing of UHMWPE surface or scratching of the metallic-femoral-head caused by loose third-body particles. The third-body particles could be bone chips, bone-cement or metallic debris trapped between the surfaces of the bearing and the femoral condyle (Wang, 2001). Adhesive wear occurs when the asperities on the articulating surface (typically the UHMWPE) are sheared off. In order for this to occur, the interfacial shear strength must be greater than the bulk shear strength of the material (Bragdon *et al.*,

1996). Fatigue wear occurs through the initiation and propagation of surface or subsurface cracks under cyclic loading conditions (Wang, 2001).

Table 2-1. Causes of TKR failure.

Reference	Average Follow-up Period	Failures (Percentage)	Failure Causes
Ranawat and Boachie-Adjei (1988)	9.5 yrs.	5 (5.9%)	1 loose tibial comp., 1 loose patellar comp., 1 infection
Scuderi et al. (1989)	15 yrs.	12 (9.4%)	4 loose tibial comp., 2 loose femoral comp., 3 infections
Kristenson et al. (1992)	10 yrs.	8 (11%)	2 loose components, 5 infections
Cadambi et al. (1994)	4.5 yrs.	30 (11.1%)	osteolysis
Diduch et al. (1997)	8 yrs.	5 (4.6%)	1 bearing wear, 2 infection
Font-Rodriguez et al. (1997)	7-21 yrs.	57 (2.2%)	3 comp. instabilities, 10 loose tibial comp., 15 loose femoral comp., 24 infections
Duffy et al. (1998)	13 yrs.	2 (2.7%)	1 bearing wear, 1 osteolysis
Van Loon et al. (2000)	12 yrs.	11 (11%)	4 bearing wear, 2 malposition, 1 persistent pain, 4 infections
Beuchel et al. (2001)	20 yrs.	28 (7.5%)	1 condylar fracture, 1 loose femoral comp. 2 loose tibial comp., 5 bearing dislocations, 9 bearing wear, 3 ligament instability, 4 deep infection, 3 osteolysis
Laskin (2001)	10 yrs.	4 (4%)	2 ligament instabilities, 2 infections
Meding et al. (2001)	10 yrs.	9 (2.3%)	8 loose patellar comp., 1 infection
Pavone et al. (2001)	23 yrs.	10 (8.3%)	4 osteolysis, 1 perioprosthetic fracture, 2 perisstent pain, 3 infections
Sextro et al. (2001)	16 yrs.	13 (7.7%)	1 condylar fracture, 1 instability, 2 loose tibial comp., 1 loose femoral comp., 4 bearing wear, 4 loose patellar comp.
Tayot et al. (2001)	11.5 yrs.	25 (7.5%)	10 loose components, 15 infections

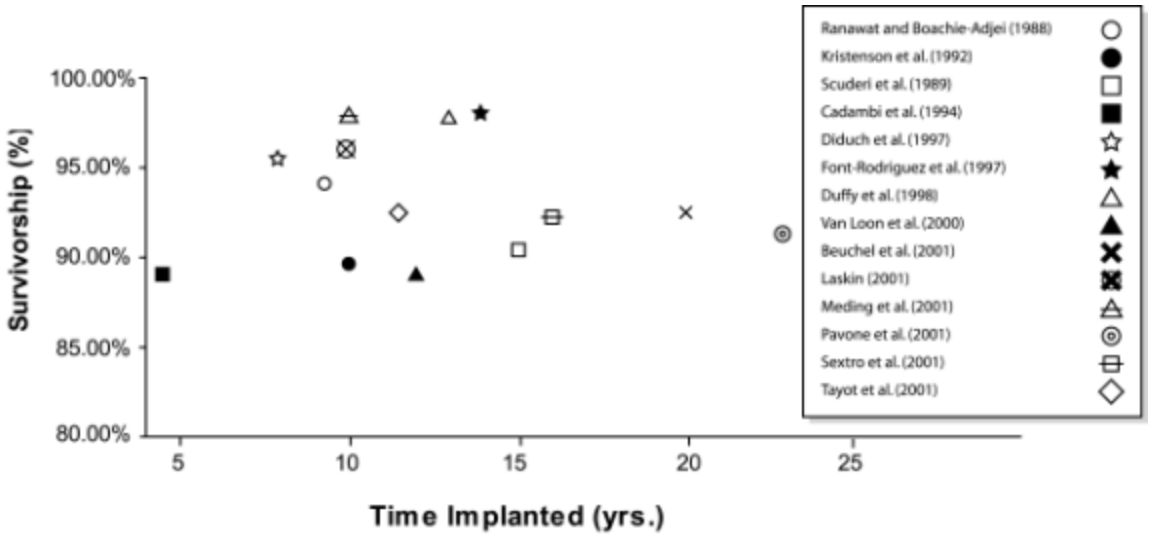

Figure 2-2: Percentage of failures in TKRs vs. years implanted.

Although wear can occur in many ways, the results of wear are similar, namely, debris is released from the articulating surface into the surrounding environment. The effect of the debris *in vivo* has been studied extensively (Hahn *et al.*, 1996; Howling *et al.*, 2001). Both of these studies linked UHMWPE wear debris found in the fluid and tissue surrounding the joint to osteolysis. Wear debris in TKRs ranges in size from sub-micron to tens-of-microns, but Howling *et al.* characterized particles less than one-micron in size as the most "biologically active." Wolfarth *et al.* also made a connection between sub-micron-sized particles and osteolysis in their 1996 study of UHMWPE particles in the synovia and tissue surrounding the knee.

The search for a polymer capable of withstanding the harsh conditions of the knee joint resulted in the discovery of ultra-high molecular-weight polyethylene. UHMWPE is a polymer characterized by long molecular chains, resulting in an 'ultra-high' molecular weight. The chains in the polymer are not typically interconnected with extremely strong bonds allowing the polymer chains to orient themselves in the direction of sliding. By

doing this, the wear resistance of the material increases and makes the polymer a valuable solid lubricant. This characteristic also creates a problem for the material when exposed to multidirectional sliding. When the chains orient themselves in the direction of sliding it makes them more susceptible to breaking from motion perpendicular to the sliding direction. The issue of multidirectional sliding was addressed by Bragdon *et al*. (1996) and Wang (2001). In Wang's 'unified theory', he compared wear rates for UHMWPE created by linear reciprocating to those from clinically retrieved prostheses. The clinical retrievals displayed wear rates one to two orders of magnitude greater than those predicted by linear reciprocating.

An innovation in the processing of UHMWPE which came about specifically to combat the effects of multidirectional sliding was improved cross-linking. Cross-linking in UHMWPE is the connection between two adjacent polymer chains via covalent C-C bonds. Increasing the density of these covalent bonds between chains prevents chain mobility and orientation as well as increasing the difficulty of breaking one chain from another. Higher cross-link density has been shown to decrease wear rates in multidirectional sliding (Wang, 2001). There are several ways to control the cross-link density, mainly irradiation followed by heat treatment is used. By irradiating the material carbon bonds are broken leaving free radicals dispersed throughout the polymer. Heat-treating serves to ensure uniform cross-link density (Wang *et al.*, 1998). After the free radicals are created, the carbon is available to bond with other molecules. One issue with cross-linking is preventing other molecules from occupying the open carbon bonds. If oxygen is present during or after the polymer is processed it can diffuse through the material and bond to the newly formed free radicals. Exposure to oxygen after

processing dramatically decreases the number of linking reactions (Premmath *et al.*, 1996) effectively weakening the inter-molecule strength. This oxidation can greatly reduce the wear resistance of the material. Storage of the material after treatment can also influence the degree of oxidation. If the UHMWPE is stored in an open-air environment it allows oxygen time to diffuse throughout the material preventing cross-linking from occurring. The problems with oxidation lead to processing and storing UHMWPE in an inert environment leaving many free radicals in the polymer un-bonded. While oxidation can occur in the body (Premnath *et al.*, 1996), the degree of oxidation is greatly reduced by preventing oxidation until the component is implanted.

Debris particle generation of UHMWPE remains a clinical issue in total joint replacements such as knees and hips. Significant advances in modeling and understanding the origin of wear debris liberation in total hip replacements have been made over the past decade. One aspect recently discovered is the importance of sliding direction on wear in UHMWPE (Bragdon *et al.*, 1996; Muratoglu *et al.*, 1999; Burroughs and Blanchet, 2001; Wang, 2001). Orders of magnitude changes in wear rate with increasing degrees of crossing motion have been reported.

Linear reciprocation is motion in one direction. Since UHMWPE has the ability to orient itself in a particular sliding direction, it can accommodate unidirectional motion very effectively. Conversely, when sliding direction is varied, UHMWPE can exhibit wear rates two to three orders of magnitude greater than linear tests find (Wang, 2001). As mentioned above, several groups have researched the effects of multidirectional sliding. The focus of these papers was motion in hip replacements, because of the hip replacement's conforming design is conducive to multidirectional motion. In the study

by Bragdon (1996) they found that an increase in the variation of sliding direction increased the wear rates demonstrated by the UHMWPE. Although Wang's study was similar, he went a step further and tried to quantify the degree of multidirectional motion by defining an angle alpha. Wang used this angle to measure degree of multidirectionality and showed increase in the crossing angle led to an increase in wear.

The conforming and axis-symmetric nature of hip joint replacements has facilitated the study of their relative motion for fluid mechanics and lubrication (Meyer and Tichy, 1999) and contact studies (Bragdon *et al.*, 1996; Maxian *et al.*, 1996; Wang, 2001; Kurtz *et al.*, 1999). To date, the complexity of the knee motions has prevented detailed study of the tibial component. Locus plots, which seek to represent the kinematics by following the most probable locations of contact on the tibial component, do not capture the relative motions experienced by a particular location on the surface. To capture this information it is critical to model the pressure distribution (which spans multiple surface elements) and the slip velocity over an entire activity cycle tracking the contact conditions for each surface element.

In order to accurately depict the motions in a knee joint during patient activity Scott Banks and Andrew Hodge (1996) developed a method for imaging the components *in vivo* known as video fluoroscopy. This method is used to determine the kinematics of TKR components throughout a variety of exercises. To accomplish this, Banks and Hodge took x-rays of the patients at discrete time intervals during the motion, and compared the component outlines with predefined libraries of component positions. The image comparison was made using Fourier transforms of the shapes. The results were data files containing the relative position of the origin of the femoral condyle with respect

to the tibial bearing's origin, as well as, the orientation of the axes of the femoral condyle's coordinate system with respect to the axes of the bearing's system. This technique has since been used in other studies of knee positioning (Asano *et al.*, 2001; Hoff *et al.*, 1998)

Other groups have tried to accurately reproduce the motions of the knee. Chen *et al.* (2001) developed a computational technique to determine preoperatively the kinematics of a knee replacement design. The program was validated using a theoretical symmetric knee, so any motion in the medial-lateral direction would be shown as erroneous. This was not the only attempt to use technology to estimate *in vivo* motions. Godest *et al*. (2002) used computational models to estimate the motions in a knee using models of muscles and ligaments as well as Finite Element Analysis (FEA) to determine feasible pressure distributions. The result was pressures ranging from 17 to 22 MPa depending on the mesh size and angles accurate to $\pm 15\%$.

The ability to accurately predict pressure distributions on the surface of the tibial component depends on the simulations' capability of reproducing muscle and ligament forces in the knee accurately. Forces experienced by the knee joint during motions are not clearly defined to date. While many studies have focused on estimating the forces in the muscles, tendons, ligaments etc., there is yet to be a perfect solution. The reason for this is the complexity of the tissue surrounding the knee joint. Not only the muscles which move the legs, but the tendons and ligaments which hold the joint together must be accounted for in modeling of the system. Costigan *et al* (2002) studied the gait and stair cycles of 35 patients to estimate the kinetics of the knee during these motions. The study reported maximum contact forces in the distal-proximal direction ranging from 3 to 6

times bodyweight. Because the instrumentation of a knee *in vivo* is not feasible at this time many studies have focused on developing models for the various tissues surrounding the knee (Seireg and Arvikar, 2001; Mikosz *et al.,* 2000; Komistek *et al.,* 2000). Seireg and Arvikar used a linear springs method to model the muscle and bone forces in the knee and found maximum force values of six times body weight. This result is supported by the study by Costigan *et al*. (2002). Another solution incorporating the springs method was Mikosz *et al*. who modeled 13 muscles and various tendons and ligaments to find a solution for knee forces. Their solution was compared to EMG readings, which approximate muscle forces, and was validated as a first-order approximation. Komistek *et al* incorporated Kane's method of dynamics into a model of the lower extremity. This study modeled forces from muscles, ligaments and tendons in the ankle, knee and hip joints. The solution required solving 30 equations with as many unknowns, for several predetermined positions. The results were compared to available video-fluoroscopy data.

Temperature rise in total hip joint replacements as a result of frictional energy being dissipated at the contact has been measured *in vivo* (Bergmann *et al.,* 2001a), *in vitro* (Liao *et al.,* 2002), and has been modeled using 2-d and 3-d finite element techniques (Hu *et al.,* 2001, and Bergmann *et al.,* 2001b, respectively). In the main, the studies conclude that frictional heating may cause temperature rises on the order of 1-10°C, and that low friction implant materials are the best way to reduce frictional heating.

Kurtz *et al*. (2002) reviewed the thermomechanical behavior of UHMWPE. It was shown that thermal processing, primarily used to increase oxidation resistance, significantly changed the mechanical behavior of the UHMWPE. Kurtz also determined that environmental temperatures between $20^{\circ}C$ and $60^{\circ}C$ do affect mechanical

properties of the polymer, but they can be "accurately predicted using an Arrhenius model. . . ."

Young *et al.* investigated the effect of heat generated by friction in the knee joint. It was determined that frictional heating caused temperature rise at the surface, but due to cooling provided *in vivo* by synovial fluid the subsurface experienced the highest temperature rise. Modeling of the bearing yielded a maximum temperature rise below the surface 1 to 2 mm. This distance corresponds to a maximum subsurface shear stress, and the combination of the two could result in higher wear for the prosthesis. The authors conclude that reduction in frictional heating would increase the functional life of a TKR.

Bergmann, Graichen, Rohlmann, Verdonschot and van Lenthe (2001) studied temperature rise in hip replacements *in vivo.* Data was recorded from instrumented components using telemetry. The patients were studied during gait and cycling activities. Maximum-recorded temperature was $43.1^{\circ}C$ after one-hour of walking. The temperatures for cycling were lower than gait indicating that normal load had a large influence on the heat produced. This conclusion is supported by the equation for power produced from frictional heating:

$$P \propto mF_N V \qquad 2.1$$

The group also published a follow-up paper using FEA to determine the sensitivity of temperature rises to materials considered for the prostheses. Material properties of the femoral-head in the replacement were shown to affect the thermal state e.g. a cobalt-chromium head resulted in temperatures in the synovia of $46^{\circ}C$.

Hu *et al.* (2001) studied the affect of temperature rise in total hip replacements. The thermomechanical finite-element simulation showed temperature rise in the hip to be

significant in changing the properties of the polymer. The maximum temperature seen in the simulations was $42.9^{\circ}C\left(110^{\circ}F\right)$, this occurred at a friction coefficient of 0.1. The results agree with experimental results produced by Bergmann *et al*. The study noted that temperature can affect wear rate, creep, fatigue and oxidative degradation. All of these factors lead to aseptic loosening of the parts and early revision surgery.

CHAPTER 3
ENGINEERING APPROACH

3.1 Experimental Data

Fluoroscopic kinematic data were collected from one total knee arthroplasty patient: female, age 65 at time of surgery, height 170 cm, mass 70 kg (Harman *et al.*, 2001). The implanted component was a cemented posterior-cruciate ligament retaining prosthesis (Series 7000, Stryker Howmedica Osteonics, Inc, Allendale, NJ) with a 6.8 mm thick insert. The Knee Society Clinical Rating System scores for this patient (Insall *et al.*, 1989) were 97-knee and 80-function after one year and 99-knee and 100-function after two years. The collected kinematics of this implant and patient are shown in Figure 3-1, with a locus plot describing the path of the contact pressure centroid over the insert for the various activities.

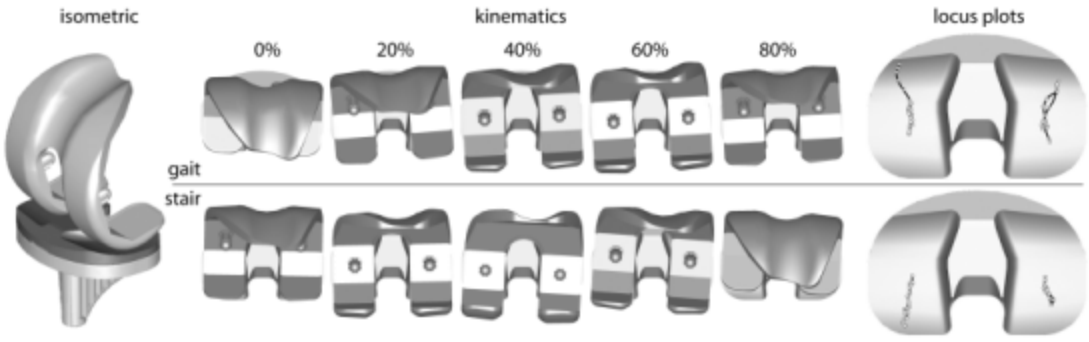

Figure 3-1: Component design and film strips of the kinematics for the gait and stair rise activities, the corresponding locus plots of contact pressure centroid is shown to the far right.

The patient performed treadmill gait and stair rise/descent activities during fluoroscopic motion analysis (Banks, 1992; Banks and Hodge, 1996; Banks *et al.*, 1997a, Banks *et al.*, 1997b) 21 months after surgery. Fluoroscopic analysis matches three-dimensional geometric models of the prosthetic components to the two-dimensional fluoroscopic images. The technique is accurate to approximately 1° for all rotations and 0.5 mm for translations in the sagittal plane (Banks and Hodge, 1996). Kinematic data from one representative cycle of each activity was averaged in 5° increments of knee flexion for stair and 1% increments for gait including stance and swing phases.

A dynamic simulation of the patient's *in vivo* knee mechanics was created by incorporating an elastic contact model into a commercial multibody dynamics software program (Fregly, Sawyer, Banks and Harman, 2002)(Pro/MECHANICA MOTION, Parametric Technology Corporation, Waltham, MA). This approach was taken to predict joint kinematics and contact pressures in a fraction of the time possible with current dynamic finite element methods (Giddings *et al.*, 2001; Godest *et al.*, 2002). The contact model uses elastic foundation theory (Johnson, 1985; An *et al.*, 1990; Blankevoort *et al.*, 1991; Li *et al.*, 1997) and treats the tibial insert as an elastic layer contacting a rigid femoral component. This model formulation accommodates the finite thickness and dimensions of the tibial insert, conformal or non-conformal contact situations, and linear or nonlinear polyethylene material properties. The elastic contact model was implemented as a dynamic link library that can be incorporated into any multibody dynamics software.

The elastic foundation approach calculates contact pressures on a grid of elements covering the tibial insert contact surfaces. The elements define a "bed of springs" where

each spring is independent from its neighbors (Johnson, 1985). This approximation eliminates the integral nature of contact problems, thereby greatly simplifying the analysis of conformal geometry or nonlinear materials. For any element, given the interpenetration d between the undeformed tibial and femoral surfaces in the direction of the local surface normal, the contact pressure p acting on the element can be calculated from (Johnson, 1985; An *et al.*, 1990; Blankevoort *et al.*, 1991).

$$p = \frac{(1-n)E}{((1+n)(1-2n))h}d \qquad 3.1$$

where E is Young's modulus of the elastic layer, n is Poisson's ratio of the elastic layer, and h is the layer thickness at that location. The interpenetration d for each element is calculated using the ACIS 3D Toolkit (Spatial Corporation, Westminster, CO). For a nonlinear material, E can be defined as a nonlinear function of p (Cripton, 1993), in which case Eqn 3.1 becomes a nonlinear equation in p that can be solved using standard root-finding methods (Nuño and Ahmed, 2001). To produce a set of point forces, the resulting element pressures are multiplied by their corresponding areas. These forces are replaced with a single equivalent force and torque applied to both bodies for purposes of dynamic simulation (Kane and Levinson, 1985).

The dynamic contact model used *in vivo* fluoroscopic measurements (anterior-posterior translation, internal-external rotation, and flexion; Fig. 3-2 a, b, and c, respectively) as prescribed kinematic inputs. The model predicted the remaining degrees of freedom (axial translation, varus-valgus rotation, and medial-lateral translation) via forward dynamic simulation to ensure compatibility with the applied loads. All prescribed and predicted motions were for the femur moving with respect to a fixed tibia.

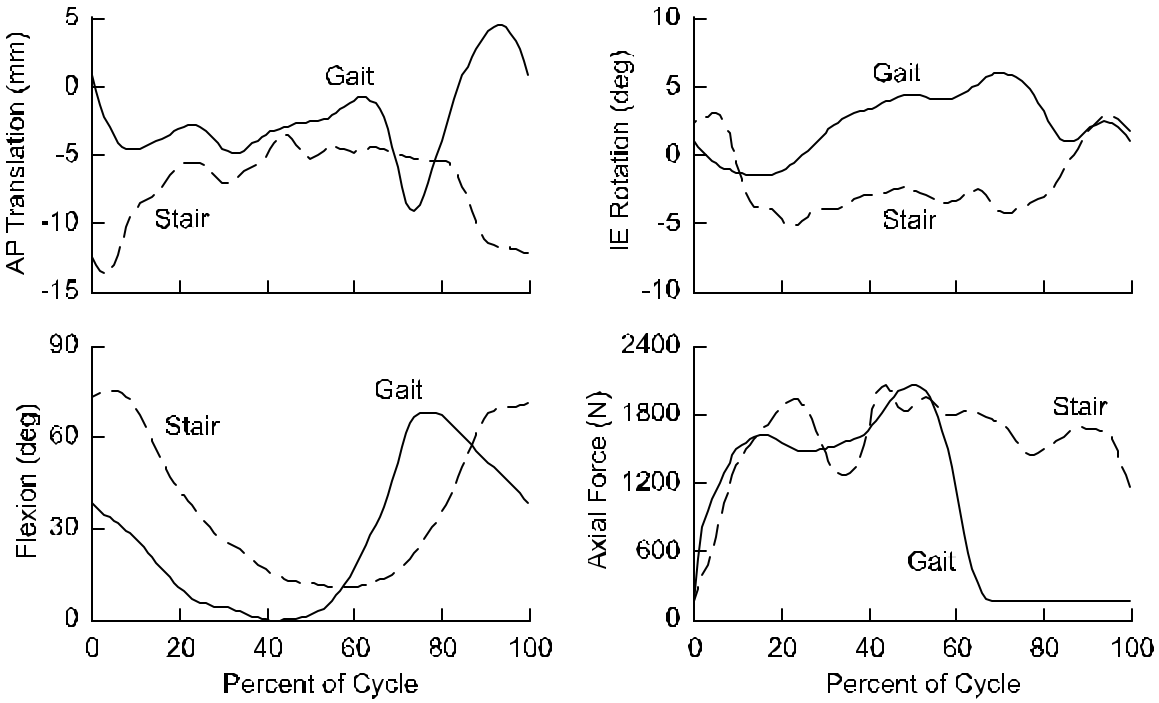

Figure 3-2: In vivo experimental data used as inputs to the dynamic contact model. a)Anterior-posterior (AP) translation. b) Internal-external (IE) rotation. c) Flexion. d) Axial force. Kinematic data are from pre-retrieval video fluoroscopy gait and stair experiments with the femur moving with respect to the tibia. Anterior translation and external rotation are positive. Axial force data are scaled vertical ground reaction force data from a patient of similar age, height, weight, and knee flexion characteristics.

Calculation of accurate slip velocities and contact pressures on individual surface elements requires the dimensions of the simulated contact patch to match *in vivo* conditions. The ability of the elastic foundation contact model to predict contact areas and pressures was evaluated experimentally using 16 different static loading conditions (loads of 750, 1500, 2250, and 3000 N and flexion angles of 0, 30, 60, and 90). For each condition, experimental pressure measurements were made with a Tekscan K-Scan sensor. Using linear polyethylene material properties, the model was able to predict experimentally measured average contact pressures to within 0.3 ± 0.5 MPa, indicating that the contact areas were also well predicted. Predictions made using nonlinear material

properties were less accurate. Consequently, a linear rather than nonlinear polyethylene material model was used in the present study.

Dynamic simulations, representing patient-specific *in vivo* conditions, were generated by combining *in vivo* fluoroscopic measurements with assumed loading conditions. In the dynamic contact model, the femoral component possessed six degrees of freedom (DOFs) relative to the tibial insert. Three DOFs (anterior-posterior translation, internal-external rotation, and flexion) were defined to match fluoroscopically measured gait and stair kinematics (two separate simulations). The remaining three DOFs (axial translation, varus-valgus rotation, and medial-lateral translation) were numerically integrated to predict their motion. An axial force was applied vertically downward to the femoral component to produce a 70% medial-30% lateral load split at 0º flexion (Johnson *et al.*, 1981; Schipplein and Andriacchi, 1991; Hurwitz *et al.*, 1998). The axial force curve for each activity was defined by scaling a vertical ground reaction force curve (Lu *et al.*, 1997; Taylor *et al.*, 1998, Taylor and Walker, 2001) to be between 0.25 and 3.0 BW (Schipplein and Andriacchi, 1991; Lu *et al.*, 1997; Taylor *et al.*, 1998, Taylor and Walker, 2001). Ground reaction force data were taken from a patient of similar age, height, weight, and knee flexion characteristics.

The dynamic contact model generated contact pressures and slip velocities in two steps. First, a forward dynamics simulation calculated contact forces and kinematics. Then an inverse dynamics analysis used the results from the forward dynamics simulation to calculate contact pressures and slip velocities over a 50x50 element grid on each tibial contact surface.

3.2 Mathematics

A computational wear model was developed to produce element-by-element damage predictions given the calculated time history of contact pressures and slip velocities experienced by each element. The model computes total damage depth for each element as the sum of material removal due to mild wear and surface deformation due to compressive creep:

$$d_{Damage} = N \cdot d_{Wear} + d_{Creep} \qquad \textit{Eqn } 3.2$$

where d_{Damage} is the total damage, d_{Wear} is the damage per cycle due to mild wear, N is the total number of cycles, and d_{Creep} is the damage due to creep. The number of cycles was based on the number of months implanted assuming 1 million cycles per year of gait or stair (Schmalzried *et al.*, 1998).

Wear predictions were made in the software using Archard's wear model for mild wear (Archard and Hirst, 1956). The model predicts the wear depth at a point on the surface of a sliding contact based on the contact pressure, sliding distance and the wear rate:

$$d_{Wear} = k\sum_{i=1}^{n} p_i d_i = k\sum_{i=1}^{n} p_i \left|v_i\right| \Delta t \qquad \text{Eqn } 3.3$$

where k is the wear rate $\left(mm^3/Nm\right)$, p_i is the contact pressure (MPa) and the sliding distance is calculated as the product of the slip velocity magnitude $\left|v_i\right|$ (m/s) multiplied by the time increment Δt (s). The appropriate value of wear rate was based on surface roughness values measured from contacting areas of the retrieved femoral component. The measurements were made using a white-light optical interferometer

(Wyko NT1000, Veeco Instruments, Woodbury, NY). Multiple locations on the surface yielded results varying from 46 to 275 nm with an average value of 131 nm. Fisher *et al.* (1994) published wear rates for UHMWPE, subjected to similar contact conditions, as a function of R_a. Based on the average R_a value, a wear rate of $k = 220\times10^{-9}\ mm^3/Nm$ was chosen.

Ultra-high molecular-weight polyethylene is a viscoelastic and viscoplastic material, as such it deforms in a time-dependent manner when stressed (Waldman and Bryant, 1997; Lee and Pienkowski, 1998). This characteristic of the polymer is responsible for some portion of surface deformation and must be accounted for. Creep characteristics for medical grade UHMWPE have been published by Lee and Pienkowski (1998). According to their research, compressive creep can be estimated as a function of time of compression and contact pressure using the following model:

$$d_{Creep} = \left[3.491\times10^{-3} + 7.996\times10^{-4} \left(Log\left(N\sum_{i=1}^{n}\Delta t_{ci} \right) - 4 \right) \right] \frac{\sum_{i=1}^{n} p_{ci}}{\sum_{i=1}^{n}\Delta t_{ci}} h \qquad 3.4$$

where all notation is previously defined with the exception of the subscript c indicating instances in time when the surface pressure p_i is non-zero, and h the initial thickness of the tibial insert. The model assumes pressures are in MPa and time has units of minutes. The resulting deformation has units matching the units of bearing thickness e.g. bearing thickness in mm yields deformations in mm.

The thermal modeling begins by assuming a particular partitioning of energy Q (J) into the femoral component Q_f and tibial component Q_t respectively. Eqn 3.5 gives an expression for the energy dissipated in the contact, where m is the friction coefficient, F

is the normal load, V is the slip speed, T is the total activity time, and t is an instant in time during the activity.

$$Q = Q_f + Q_t = m\int_0^T F_t \left|V_t\right| dt \qquad 3.5$$

The energy is partitioned into the two bodies as shown in Figure 3-3 and given by Eqn 3.6. The energy partition rule is based on matching the interface temperature for: (a) stationary contact area of two half-spaces, and (b) femoral component moving relative to a stationary tibial component. Both the femoral component and tibial component are modeled as half spaces of thermal conductivities k_f and k_t respectively. Partitioning heat based on a moving heat source (b) is generally preferred when the Peclet number, Pe, is greater than 10 (Williams *et al.*, 1994; Bhushan, 1999).

$$\begin{aligned} Pe<10 \quad & Q_t = Q\left(1+\frac{k_f}{k_t}\right)^{-1} \qquad Q_f = Q\left(1+\frac{k_t}{k_f}\right)^{-1} \\ Pe>10 \quad & Q_t = Q\left(1+\frac{k_f}{k_t}\frac{\sqrt{Pe_f}}{1.6}\right)^{-1} \qquad Q_f = Q\left(1+\frac{k_t}{k_f}\frac{1.6}{\sqrt{Pe_f}}\right)^{-1} \end{aligned} \qquad 3.6$$

The Peclet number for the femoral component is defined as $Pe_f = \frac{V_f l}{a_f}$, where V_f is a characteristic sliding speed of the femoral component, l is a characteristic half width of the contact patch, and a_f is the thermal diffusivity of the femoral component. From Eqn 3.6 it can readily be seen that the moving source partitions greater heat into the femoral component for $Pe_f > 10$. A stationary partitioning of heat is assumed for the remainder of the modeling and analysis, in part because partitioning greater amounts of heat into the

tibial component should provide an upper bound on the frictional heating likely to be seen in service.

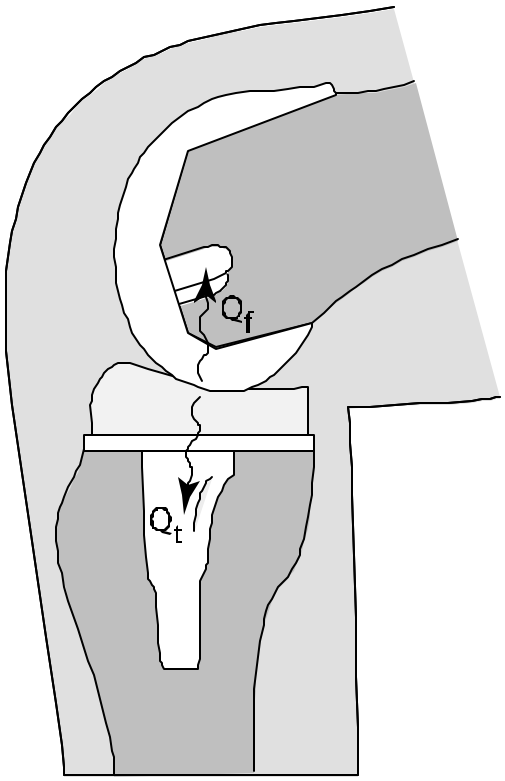

Figure 3-3: Schematic of the knee joint showing the partitioning of energy into the femoral and tibial component.

The heat flux $\dot{q}_i$ (W / m^2) is found for a tibial element i by partitioning the average energy dissipated over that element and dividing by the activity time. This is shown in Eqn 3.7, where P_t is the pressure on element i at time t.

$$\dot{q}_i = \frac{m}{T\left(1+\frac{k_f}{k_t}\right)}\int_0^T P_t |V_t| dt \qquad 3.7$$

The temperature rise q_l at a particular element l is found using the algorithm shown schematically in Figure 3-4 and given by Eqn 3.8. This algorithm is for square

elements of area A, half width a, and the vector from the origin element l to element i is $\vec{r}_{li}$.

$$q_l = 1.12\frac{\dot{q}_l a_l}{k_t} + \sum_{i=0}^{n;i\neq l}\frac{\dot{q}_i A_i}{2p\,k_t\left|\vec{r}_{li}\right|} \qquad 3.8$$

The first group in the algorithm is the central temperature rise of the square element under uniform heat flux $\dot{q}_l$. The second group in the algorithm is the summation of all of the contributions of the remaining surface elements to the temperature rise. This algorithm treats all of the contributing elements as a single point source of heat, $\dot{Q}_i = \dot{q}_i A_i$, and uses the classic point source solution discussed in detail in Carslaw and Jaeger (1959). This algorithm is used for all elements regardless of whether or not they experience a frictional heat flux.

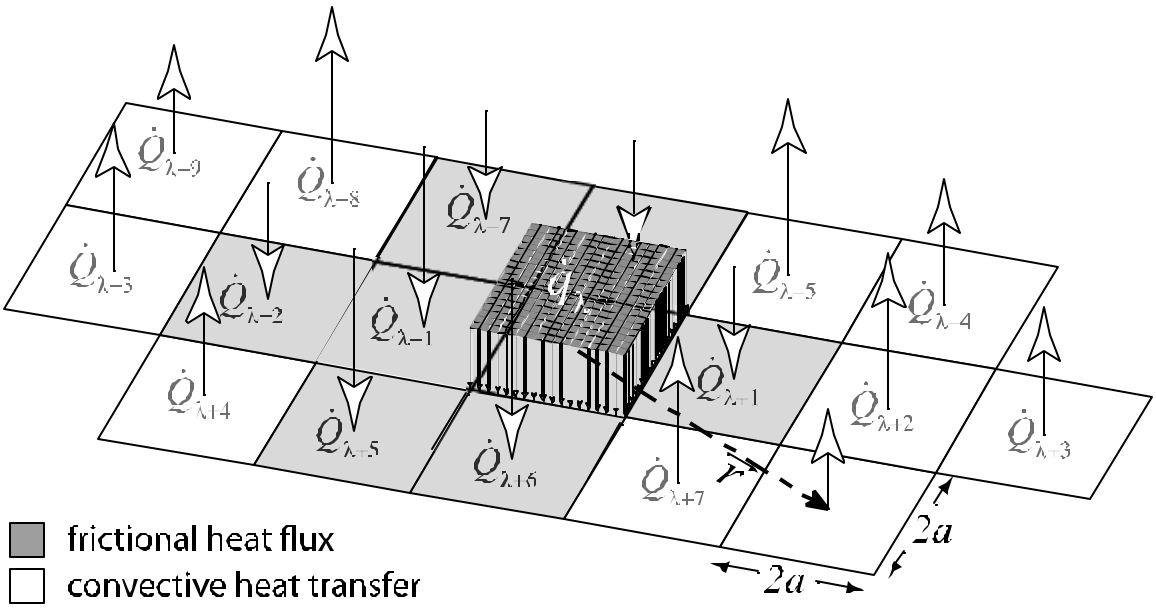

Figure 3-4: Schematic of the solution approach for temperature rise of element l, with neighboring elements treated as point sources of heat (both frictional heating and convective cooling).

The elements that do not experience a frictional heat flux during the activity are exposed to the synovial fluid, and convective cooling of the component occurs through this surface/fluid interface. The heat flux of these elements not in contact is assumed to follow Newton's law of cooling, as shown in Eqn 3.9, where q_i is the temperature rise of the element above ambient temperature $q_i = T_s - T_{amb}$ and h is the convection heat transfer coefficient with units of $W/\left(m^2 \cdot K\right)$.

$$\dot{q}_i = -hq_i \qquad 3.9$$

The solution for the surface temperature map of the tibial component requires an iterative solver due to the coupling between the convective cooling heat flux and the surface temperature. The solution approach is similar to a fixed-point iteration with two constraints on the solution method: 1) the convective cooling power cannot exceed the frictional heat, and 2) surface temperatures below ambient are not permitted.

Analysis of crossing motion occurs at the level of the individual surface elements on the tibial insert and observes the motion of the femoral component relative to each element. The only motions of interest are those that occur when the element is in contact with the femoral component, a condition of non-zero contact pressure. Following the style of presentation previously shown by (Wang, 2001) on crossing motions in hip contacts, a trimetric view of the tibial surfaces with over-laid velocity vectors for 10 representative elements is shown in Figure 2. This qualitative plot is generated from stair-rise data, which shows the greatest degree of crossing. It is shown here to illustrate the very limited degree of crossing motion seen in this design, and to illustrate the need to develop a formulaic quantitative measure of crossing intensity that can be used to visualize crossing on all the elements simultaneously.

Figure 3-5 (a) gives a vector plot of the slip velocities for 17 evenly spaced increments in time, for an element in the lateral compartment of the tibial bearing during stair rise. As can be seen from the locus plot shown in Figure 3.1 this patient showed lateral pivoting. The elements in the lateral compartment are in contact for the most number of time steps; thus, they provide the most interesting vector-plots. In Figure 3-5 (b) the x-axis, which is the medial-lateral axis, of the slip velocity plot is exaggerated by almost an order of magnitude. In the motion path plot, these slip velocities are multiplied by the time increment to give incremental displacements of the femoral component over the element. These incremental motion vectors are strung head to tail to give a motion path. In this plot the medial lateral axis is exaggerated 20 times, to the right an un-exaggerated motion path is shown. The arrow heads on the motion path plot are evenly spaced by time, and some information about sliding speed at various locations along the path can be gleaned.

Instinctively, one knows that motion in the absence of load is not damaging. Similarly, motion during lightly loaded contact imparts less energy to the surface than identical motion during a highly loaded contact. To account for this, a tribological intensity vector is defined as the product of the contact pressure (P) and the slip vector ($\vec{\boldsymbol{d}} = \vec{\boldsymbol{V}} \cdot \Delta t$), as shown by Eqn 3.10.

$$\text{tribological intensity} = P \cdot \vec{\boldsymbol{d}} \qquad 3.10$$

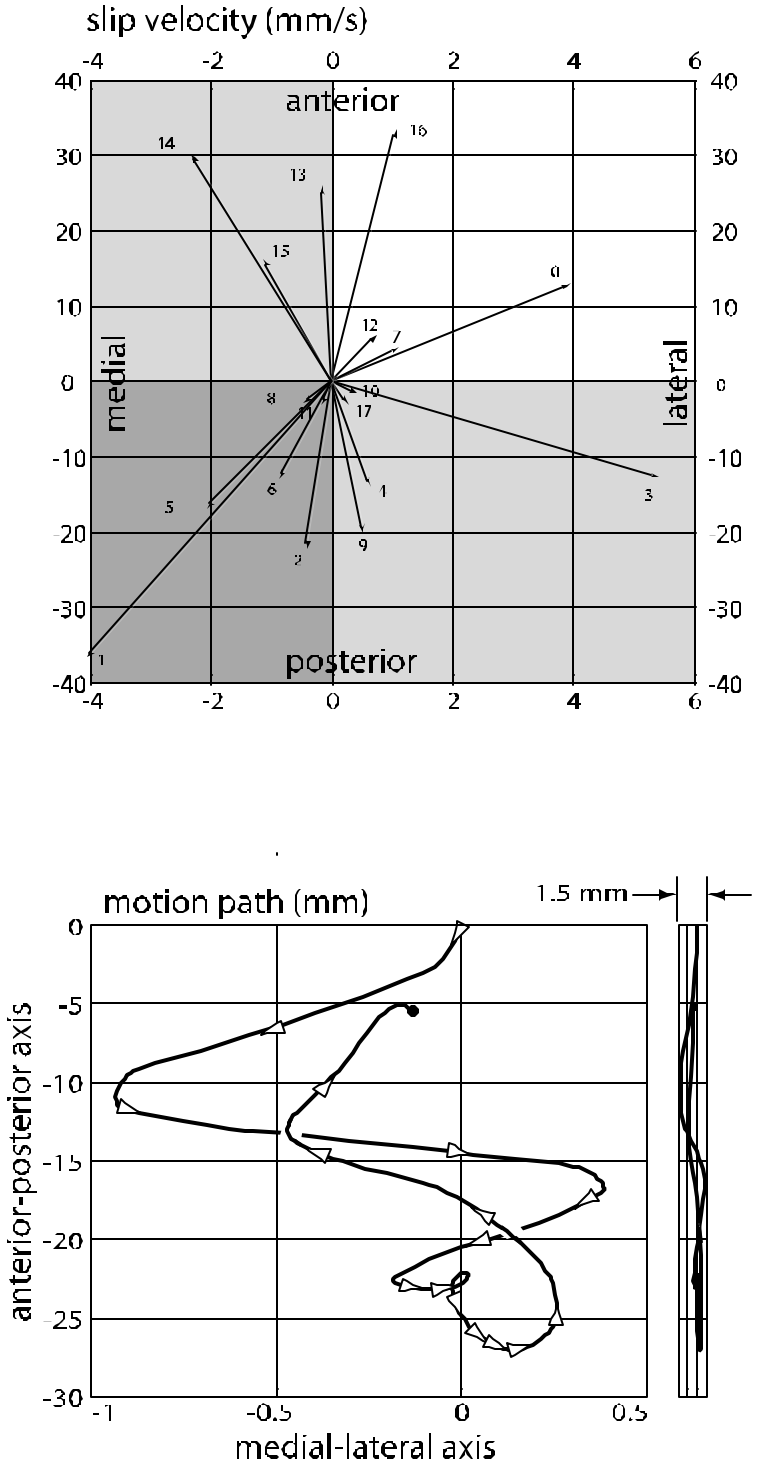

Figure 3-5: (a) Vector plot of the counterface slip velocities for 17 different instances during contact. This particular location in the lateral compartment during a stair rise activity; this location showed significant crossing motion. (b) The motion path of the femoral component over this location, notice the x-axis is exaggerated by 20 times, a 1-to-1 motion path is shown to the right.

Figure 3-6 (a) shows a vector plot of tribological intensity, with an angular coordinate (q) defined from the positive medial-lateral axis for a vector moving in the anterior direction (solid) and from the negative medial-lateral axis for a vector moving in the posterior direction (dashed). This allows all vectors to be placed on a single plot where the orientation of slip has the same angular coordinate regardless of direction, such an orientation plot is show in figure 3-6 (b). A scatter plot of tribological intensity versus angular coordinate is shown in Figure 3-6 (c). It is hypothesized that the most probable direction of polymer orientation on a particular element coincides with the dominant orientation of tribological intensity ($\bar{q}$) for that element; this is given by Eqn 3.11, where the subscript (i) denotes a particular time step.

$$\bar{q} = \frac{\sum_{i=1}^{n} q_i P_i \left|\vec{V}_i\right| \Delta t_i}{\sum_{i=1}^{n} P_i \left|\vec{V}_i\right| \Delta t_i} \qquad 3.11$$

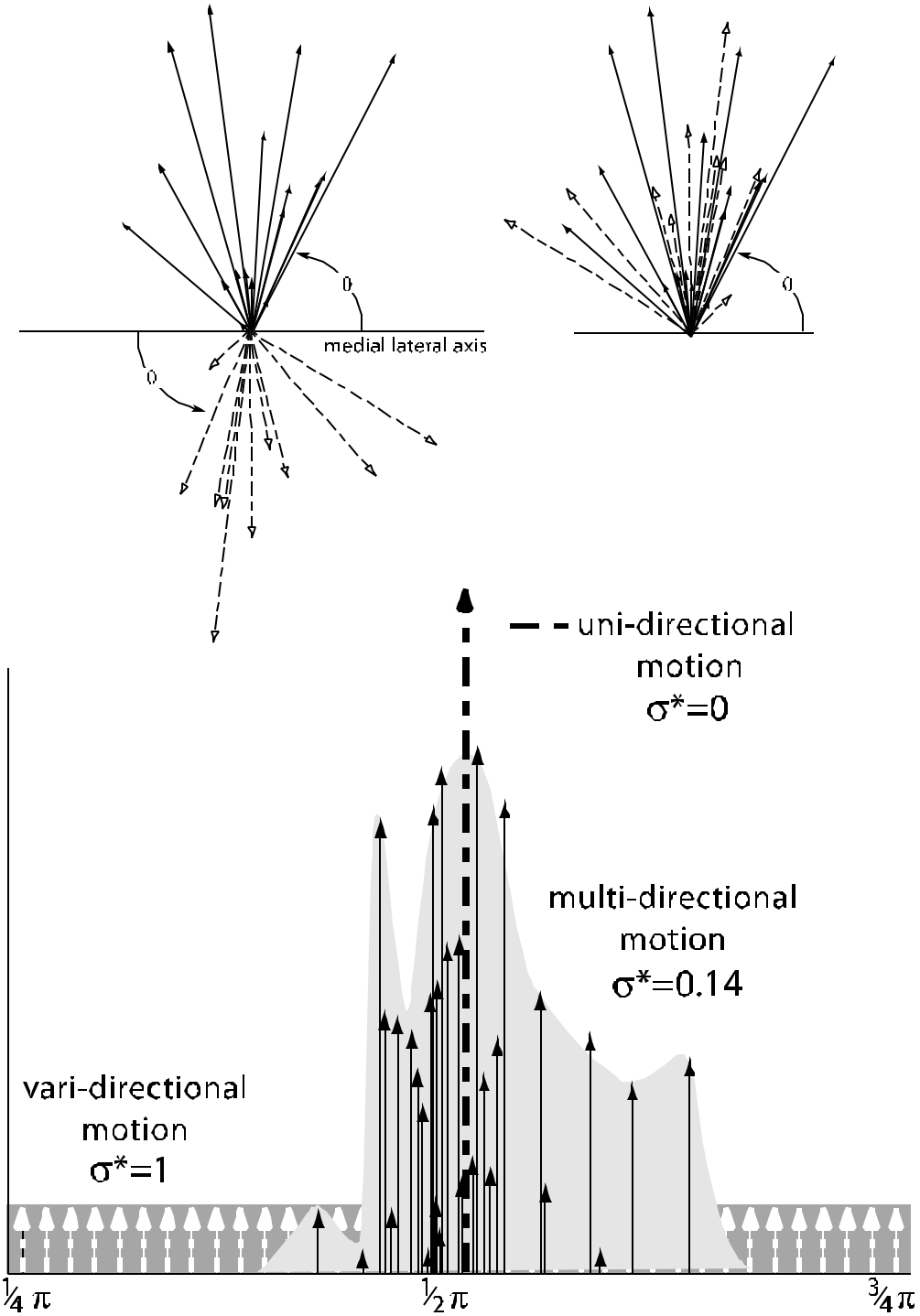

Figure 3-6: (a) Vector plot for tribological intensities shown with the angular coordinate convention (b) Overlaying plot with angular coordinate c) Scatter plot of tribological intensity versus angular coordinate compared with uni-directional motion (delta function) and vari-directional motion (step function).

As observed in laboratory tests (Burroughs and Blanchet, 2001) hip joint simulator tests (Bragdon *et al.,* 1996), and modeled (Wang, 2001; Muratoglu *et al.,* 1999) unidirectional motions produce significantly less wear than multi-directional motions. In hip and knee joints multidirectional motion arises from abduction/adduction and internal/external rotation respectively. A crossing intensity parameter (s) is defined by Eqn 3.12, and describes the spread of tribological intensity vectors about the dominant orientation direction ($\bar{q}$). This is a statistical formulation for crossing motion intensity as opposed to an extreme value parameter proposed earlier by Wang, 2001.

$$s = \sqrt{\frac{1}{n}\sum_{i=1}^{n}\left(P_i\left|\vec{V}_i\right|\Delta t_i\left(\bar{q}-q_i\right)\right)^2} \qquad 3.12$$

The crossing intensity of a circular counterface motion gives continuously varying and evenly distributed (vari-directional) tribological intensity vector orientation and is defined as s_o. This is given by Eqn 3.13, where the subscript (o) denotes vari-directional motion parameters.

$$s_o = \sqrt{\frac{1}{n}\sum_{i=1}^{n}\left(P_o\left|\vec{V}_o\right|\Delta t_o\left(\frac{p}{2}-q_i\right)\right)^2} \qquad 3.13$$

The products of slip distance and contact pressure for this vari-directional motion are constant and the summation must give the same overall tribological intensity as shown by Eqn 3.14. The normalized crossing intensity (s^*) is given by dividing the element crossing intensity (Eqn 3.12) by the equivalent vari-directional crossing intensity (Eqn 3.13), which is shown in Eqn 3.15 in terms of only element parameters.

$$P_o\left|\vec{V}_o\right|\Delta t_o = \frac{1}{n}\sum_{i=1}^{n} P_i\left|\vec{V}_i\right|\Delta t_i \qquad 3.14$$

$$s^* = \frac{s}{s_o} = \sqrt{\frac{\sum_{i=1}^{n}\left(P_i\left|\vec{V}_i\right|\Delta t_i\left(\bar{q}-q_i\right)\right)^2}{\sum_{i=1}^{n}\left(\left(\frac{1}{n}\sum_{i=1}^{n}P_i\left|\vec{V}_i\right|\Delta t_i\right)\left(\frac{p}{2}-q_i\right)\right)^2}} \qquad 3.15$$

Using Eqns 3.11 and 3.15 both the orientation direction and normalized spread of crossing motion can be found (the crossing motion intensity is defined as $s^* = 0$ for $n = 1$).

Figure 3-7 shows the algorithm visually overlaying three different motions: (a) delta function that corresponds to uni-directional motion $s^* = 0$, (b) multi-directional motion distributed about $s^* = 0.09$, and (c) vari-directional motion distributed uniformly along the angular coordinate axis $s^* = 1$. Crossing motion is often conceptualized using a bi-directional diamond pattern, where a square has a crossing angle of 90°. Figure 3-8 shows a series of simple counterface motions. The usefulness of this normalized crossing intensity parameter is immediately obvious; the circular motion gives $s^* = 1$, the reciprocating motion gives $s^* = 0$, and the narrowing diamond patterns span the range smoothly.

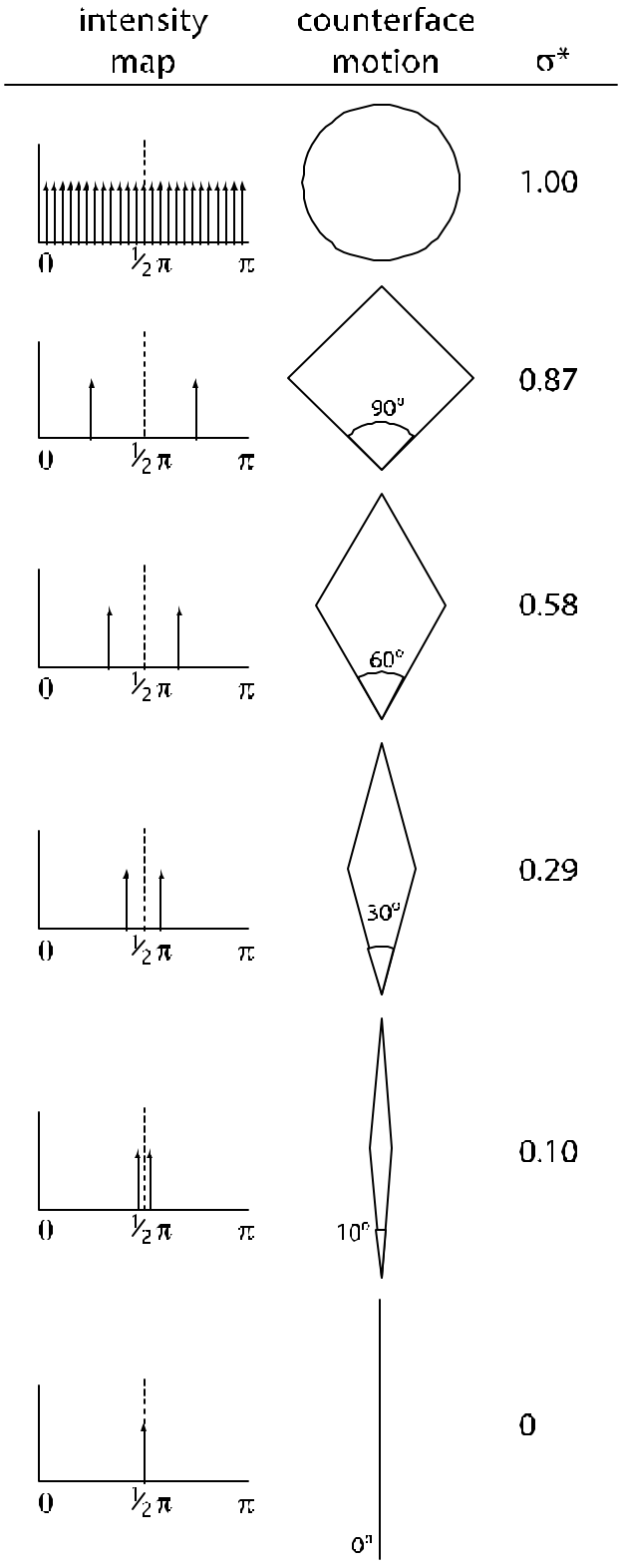

Figure 3-7: A series of simple intensity maps, with corresponding counterface motion and normalized crossing severity index.

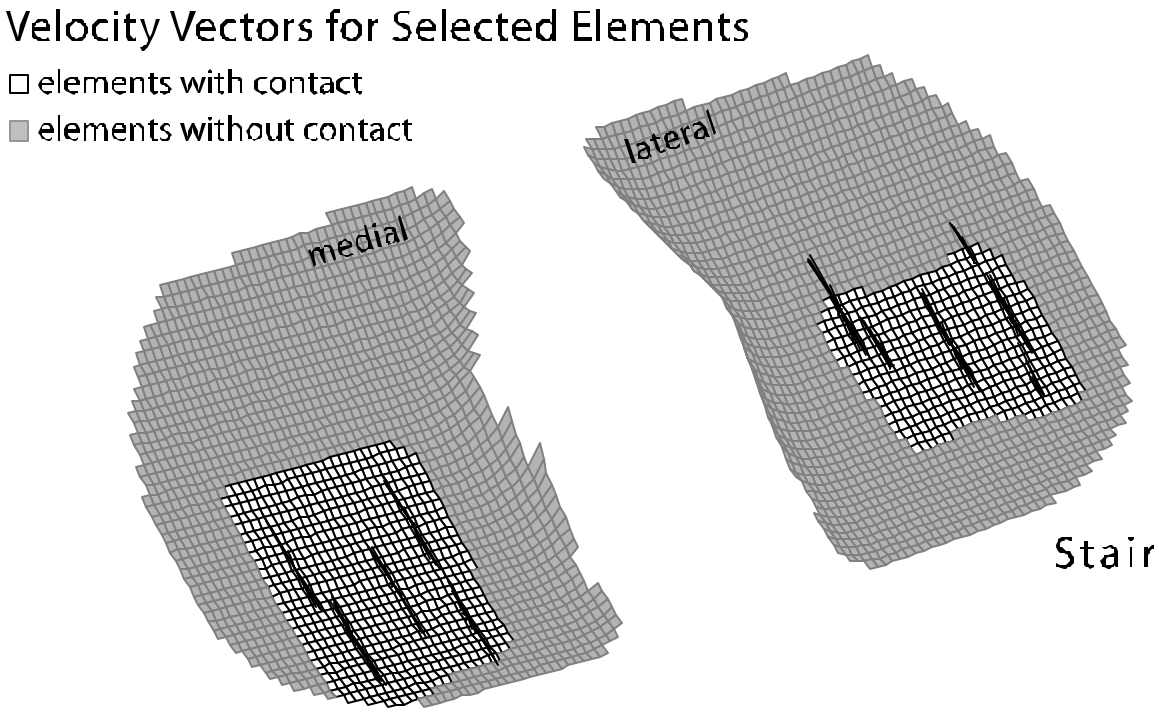

Figure 3-8: Overlaying plots of velocity vectors, normalized by the largest velocity vector in the simulation, onto the corresponding elements on the tibial mesh. These vectors are from a stair rise activity, which shows the greatest degree of crossing motion.

CHAPTER 4
RESULTS AND DISCUSSION

4.1 Wear Analysis

Five computational wear predictions (two activities with two load splits, and one partition of activities; 70% gait and 30% stair) were compared to the actual wear depths and patterns measured on the tibial insert retrieved from the patient *post-mortem*. The total time of implantation at retrieval was 51 months. For both the predictions and the retrieval, visualizations of the wear contours were generated using commercial automatic inspection software (Geomagic Qualify, Raindrop Geomagic, Research Triangle Park, NC). Using the wear predictions, the center of each contact element on the tibial insert surface was displaced by the calculated damage depth d_{Total} in the direction of the local surface normal. A "worn" polygonal surface model was created from these points, and the software generated a contour plot of the deviations between the original and worn surfaces.

The retrieval showed scratching, burnishing, and tractive striations on the articular surfaces (Harman *et al.*, 2001). Pitting and delamination were not observed. A three-dimensional scan was obtained of the worn insert (Fig. 4.1a) and a matched unworn insert using a laser scanner (Vivid 900, Minolta Corporation, Ramsey, NJ) possessing a manufacturer-reported accuracy of $\pm 0.04mm$. Once the point clouds generated by the laser scans were converted to polygonal surface models and aligned by the software, a retrieval wear contour plot was also generated (Fig. 4.1b). To determine a threshold for

reporting retrieval wear, the unworn insert was aligned with the insert CAD model and the maximum deviation between contact surfaces (0.25 mm) determined.

Qualitatively, the damage regions predicted by the computer simulations were in good agreement with the clinical wear regions (compare Fig. 4.2 with Fig. 4.1). The medial wear scars for the 70-30 gait case (Fig. 4.2a) extended along a focalized track to the anterior medial corner of the insert, similar to the retrieval. In contrast, the medial wear scars for the 70-30 (Fig. 4.2b) stair case extended broadly to the posterior rim of the insert, enlarging the region predicted by the gait cases. The lateral wear scars for the 70-30 gait case extended more anteriorly than in the retrieval, but the anterior border on the lateral side in the 70-30 stair case corresponded well with the retrieval. Altering the load split to 50-50 decreased medial damage while increasing lateral damage for both gait (Fig. 4.2c) and stair (not shown). For a 70% gait, 30% stair partitioning of activities based on linear rules of mixture, the damage area for a 70-30 load split (Fig. 4.2d) was a combination of the gait (Fig. 4.2a) and stair (Fig. 4.2b) damage areas. For both gait and stair, the lateral wear regions were more central in the anterior-posterior direction than were the medial regions, similar to the retrieval, and possessed a posterior border of extremely similar shape and location to the retrieval.

The predicted locations of maximum damage were in good agreement with the retrieval (stars in Fig. 4.1b and Fig 4.2). On the lateral side, the location of maximum damage was the same in all four simulations and was consistent with the retrieval. On the medial side, the maximum damage location was shifted toward the tibial eminence for the gait simulations (Fig. 4a and c) and posteriorly for the stair simulations (Fig. 4b). However, when a 70% gait, 30% stair partitioning of activities was considered (Fig. 4d),

the predicted maximum damage location on the medial side also became consistent with the retrieval.

Quantitatively, the simulations predicted maximum total damage depths on the same order of magnitude as those measured from the retrieved insert (Table 4-1). The predicted maximum damage depths ranged from 0.9 mm to 1.8 mm. The predicted creep deformation was approximately one-third to one-half of the total damage. The 70-30 load split for gait and stair activities exhibited approximately equal medial and lateral maximum damage depths, whereas the 50-50 load cases produced about 1.5 times deeper damage on the lateral side. Total damage area was greater for gait than for stair, while total damage volume was approximately 50% larger for stair than for gait. Smaller medial loads (50-50 split) decreased the damage volume in the medial compartment and increased damage volume in the lateral compartment such that the total damage volume was unaffected by load split.

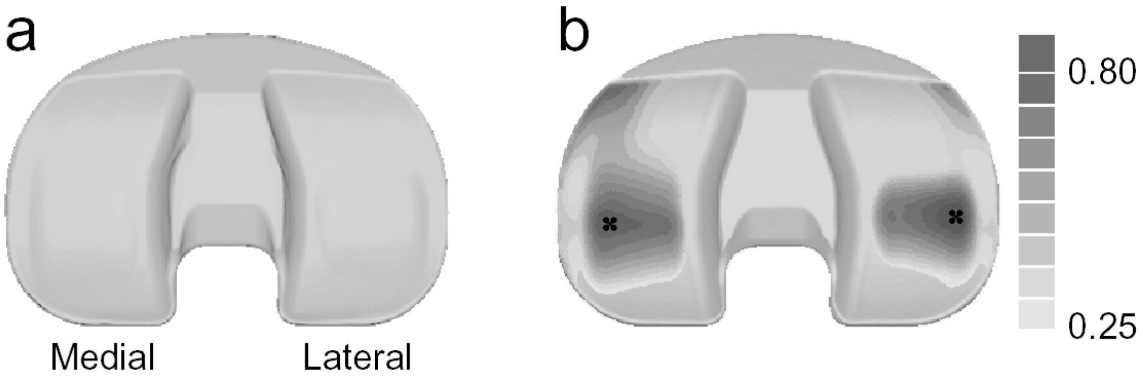

Figure 4-1: Damage visualization of the retrieved tibial insert. a) Laser scan showing damage regions visible to the naked eye. b) Contour map indicating depth of damage zones. The color bar indicates depth in mm. Stars indicate location of maximum damage on each side.

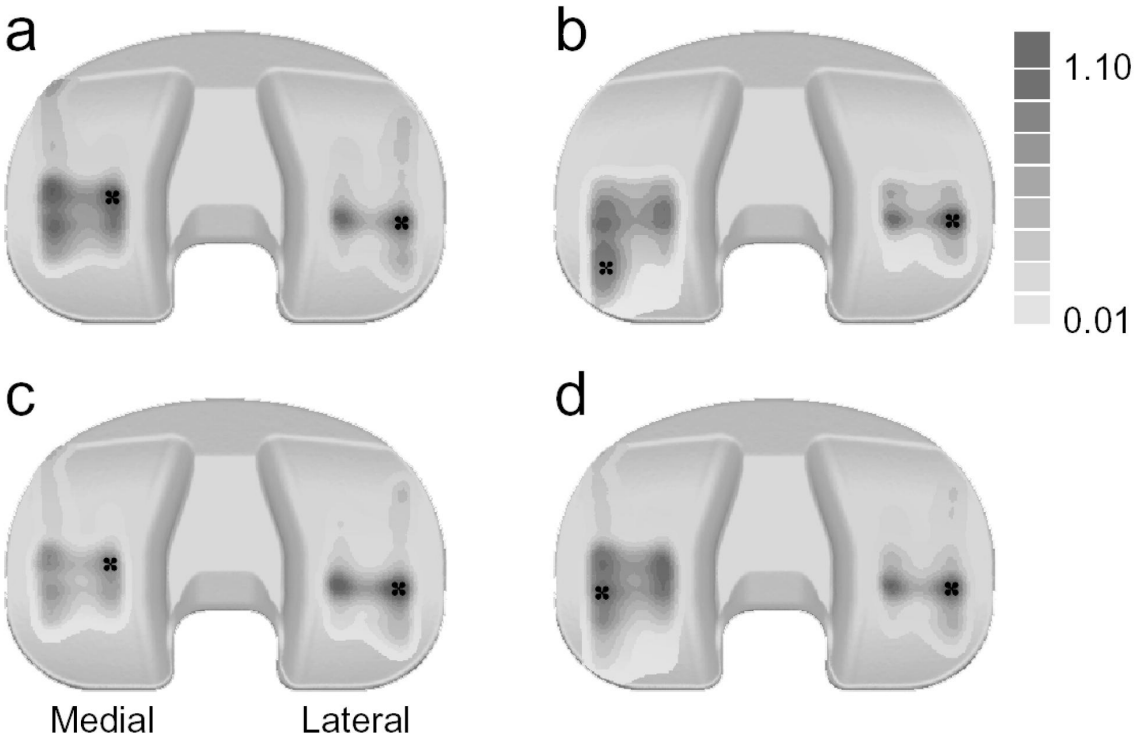

Figure 4-2: Damage contour maps predicted by the computer simulations. a) Gait with 70-30 load split. b) Stair with 70-30 load split. c) Gait with 50-50 load split. d) Combined activity assuming 70% gait, 30% stair with 70-30 load split.

Table 4-1: Quantitative summary of damage results predicted by the computer simulations for gait and stair activities with 70-30 and 50-50 load splits. Maximum wear, creep, and total damage may occur at different locations on the surface.

Load		Gait			Stair		
Split	Damage	Medial	Lateral	Total	Medial	Lateral	Total
70-30	Wear depth (mm)	0.6	0.7	—	0.7	0.8	—
	Creep depth (mm)	0.6	0.4	—	0.8	0.6	—
	Total depth (mm)	1.1	1.0	—	1.5	1.4	—
	Area (mm^2)	360	304	663	342	216	558
	Volume (mm^3)	126	57	183	204	77	282
50-50	Wear depth (mm)	0.5	0.9	—	0.6	1.1	—
	Creep depth (mm)	0.5	0.5	—	0.7	0.8	—
	Total depth (mm)	0.9	1.4	—	1.3	1.8	—
	Area (mm^2)	328	349	677	327	236	563
	Volume (mm^3)	94	89	184	152	121	273

Combining damage predictions from the two activities (70% gait, 30% stair) resulted in damage similar to the retrieved implant (Table 4-2). The predicted locations of maximum damage depth were the same as on the retrieved insert (Fig. 4-2 (d)). Maximum damage depths for the retrieval were 0.7 mm medial and 0.8 mm lateral versus 1.0 mm and 1.1 mm for the simulation. The combined case predicted 87% of the total damage area on the retrieval, 84% medially and 91% laterally. The medial-lateral ratio for damage depth was 0.88 for the retrieval and 0.89 for the simulation while for damage area it was 1.38 for the retrieval and 1.28 for the simulation.

Table 4-2: Quantitative comparison between retrieval damage and simulation damage predicted by an activity partition of 70% gait, 30% stair with a 70-30 load split.

	Retrieval[a]			Simulation[b]		
Damage	Medial	Lateral	Total	Medial	Lateral	Total
Total depth (mm)	0.7	0.8	—	1.0	1.1	—
Area (mm^2)	422	305	727	354	277	632

[a]See Harman *et al*. (2001) for measurement details.

[b]Activity partition: 70% gait, 30% stair with 70-30 load split.

Damage results predicted by the software were made using a mixture of stair and gait kinematics. Although the average person does not spend 30% of their time on stairs, the flexed-knee under high load motion performed when climbing stairs can be likened to a variety of everyday activities e.g. sitting in or rising from a chair, kneeling to tie a shoe, getting into or out of bed. While these activities are less frequent the summation of all the motions is accounted for in the 30% estimate.

Despite its computational advantages, the current contact model formulation has limitations. It does not account for viscoelastic material properties (Waldman and Bryant, 1994; Waldman and Bryant, 1997), friction (Sathasivam and Walker, 1997), or how pressure applied at one location affects the displacement of other locations (Johnson, 1985). However, the most significant issue is the use a linear material model, which explains the more focalized damage regions seen in the predictions compared to the retrieval. This material model was chosen over a nonlinear model for two reasons. First, a linear model is more in line with the guiding concept of using models with previously published, well-established parameter values. Second, in recent simulations of a different knee implant using the same dynamic contact model, a linear model matched static contact pressure measurements better than did a nonlinear material model (Cripton, 1993) for 16 different loading conditions (loads of 750, 1500, 2250, and 3000 N and flexion angles of 0, 30, 60, and 90º; Fregly *et al.*, 2002). The value of Young's modulus that reproduced the experimental data (400 MPa) was the same as the value reported by Kurtz *et al*. (2002). Use of a nonlinear material model (Cripton, 1993) in the simulations produces the same "dog-bone" contact patch (due to end effects) as the linear material model but with more uniform contact pressures across the patch (Fig. 4-3). Thus, a nonlinear material model with well-established parameter values would produce more uniform damage predictions in the medial-lateral direction, similar to the retrieval, but would not likely cause dramatic changes in the depth or distribution of predicted damage.

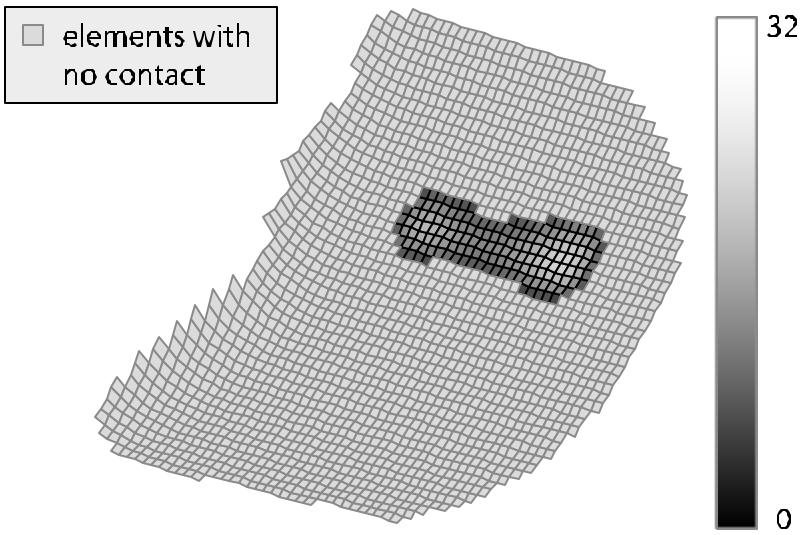

Figure 4-3: Visualization of the static contact pressures predicted by the dynamic model for an axial load of 3 BW. a) Linear material model. b) Nonlinear material model. Color bar indicates pressure in MPa. The element grid is 50 x 50, the same as that used in the damage predictions.

4.2 Crossing Analysis

The algorithms discussed in the mathematics section of Chapter 3 were applied to the patient kinematic data for two activities: gait and stair rise, and contour plots of tribological intensity and normalized crossing motion intensity were generated (figures 4-4 and 4-5). Both gait and stair activities showed limited crossing intensity, with maximum $s^* = 0.04$ and $s^* = 0.09$ respectively. The coincidence of highest crossing intensity with greatest tribological intensity occurs on the lateral compartments for both activities. This is believed to be due to the pivoting nature of this patient's kinematics.

The crossing motions observed for this patient suggest that uniform bi-directional patterns with 10° of included angle are a reasonable screening motion for pin-on-disk

testing. It is unclear how significant this degree of crossing is to the tribological behavior of the implanted UHMWPE. A model previously proposed by Wang for multidirectional sliding of UHMWPE offered a dependence of wear rate on maximum included angle ($2a$) as shown in Eqn 4.1.

$$k \propto \left(1 - \frac{\boldsymbol{sin}\, 2a}{2a}\right) \tag{4.1}$$

In the study by Wang (2001) experiments with pin-on-disk multidirectional sliding produced one order of magnitude increases in wear rate with as little as 15° of crossing motion.

Conforming knee prostheses are currently available, with designed lateral or medial pivoting. The challenges in evaluating the potential tribological impact of such designs require evaluation of both tribological intensity and crossing intensity. Perhaps, overall tribological severity is the product of the two.

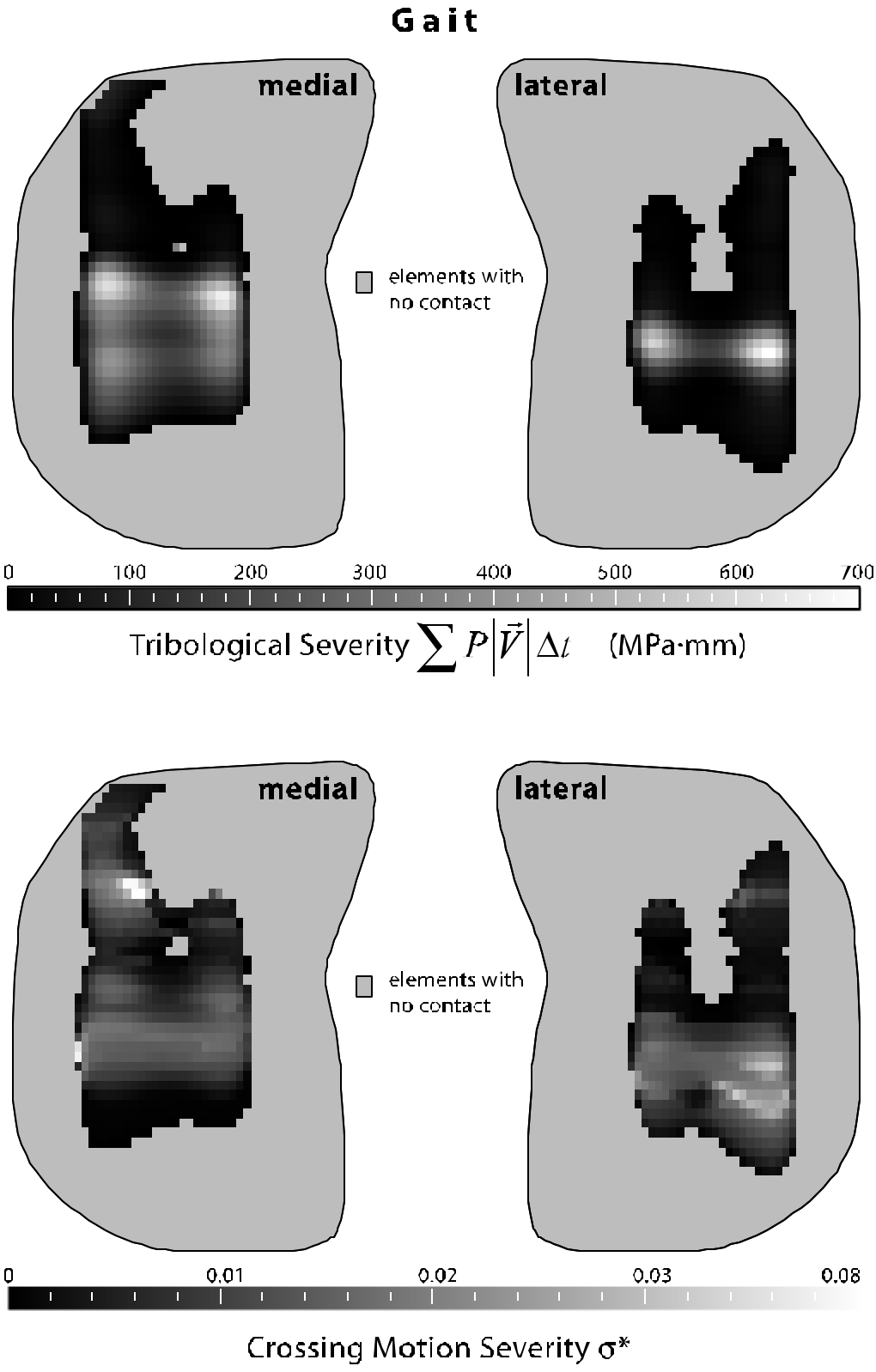

Figure 4-4: Contour maps of **a)** tribological intensity and **b)** normalized crossing severity index for elements in contact during gait.

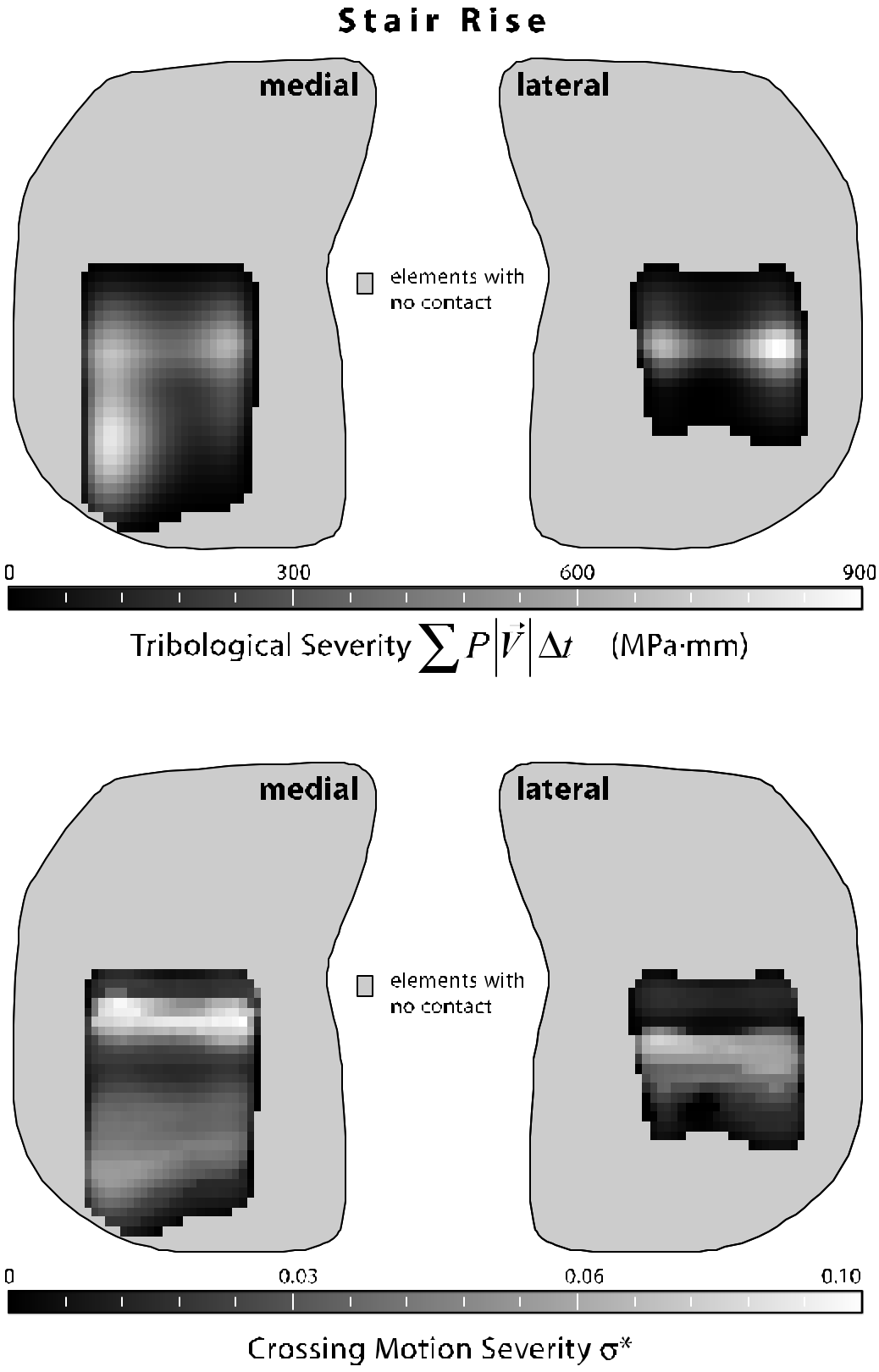

Figure 4-5: Contour maps of a) tribological intensity and b) normalized crossing severity index for elements in contact during stair rise.

4.3 Thermal Analysis

The values of the various variables needed in this code that defines the '*standard condition*' for both gait and stair rise activities are given in Table 4-3. The standard condition assumes a 1 Hz activity with a Cobalt-Chrome femoral component, a low convective heat transfer coefficient, and a low Peclet number partitioning of heat.

Table 4-3: List of standard conditions

		value	units	reference(s)
elastic modulus	E	460.	MPa	Kurtz*et al*, 2002
Poisson's ratio	ν	0.46		Bartel*et al*, 1995
thermal conductivity				
tibial component	k_t	0.4	W/(m*K)	
femoral component	k_f	13.	W/(m*K)	
convection coefficient	h	30.	W/(m^2*K)	
cycle time (stair & gait)	T	1.0	sec	Kakac and Yener, 1994
friction coefficient	μ	0.06		Hall and Unsworth, 1997

The heat flux contour plot as described by Eqn 3.7 is shown in figure 4-6 (a) and 4-7 (a) for the gait and stair activities respectively. The resulting temperature rise contour plots are shown in figure 4-6 (b) and 4-7 (b) for the gait and stair activities respectively. These temperature results converge quickly, less than 100 iterations. For both gait and stair rise activity maximum temperature occurs on the medial compartment.

The code was run varying three different parameters off of the standard condition; these were activity frequency, heat transfer coefficient, and thermal conductivity of the femoral component. Table 4-4 summarizes these data.

The choice of femoral component thermal conductivity for the standard condition corresponds to a cobalt-chrome component, which is widely used. The maximum contact temperature is extremely sensitive to the choice of femoral component thermal conductivity. At $k_f = 0.4$ half of the frictional heating is carried away by the femoral component and half goes in the tibial component. At $k_f = 40.0$ only 1% of the frictional heating goes into the tibial component.

The stationary analysis partitions heat to the respective bodies as a function of their thermal conductivities only. This is considered reasonable for low values of Peclet number. However, for the standard condition (Cobalt-Chrome femoral component) characteristic sliding speed is $Vf = 0.100\ m/s$, representative contact half-length is $l = 0.002\ m$, and the thermal diffusivity is $a_f = 3.4x10^{-6}$, thus $Pe_f \approx 60$. The energy partition and corresponding maximum temperature rise for this standard condition is $Q_t = 3\%\ Q_{total}$ & $q_{\max} = 10.5^o C$ and $Q_t = 0.6\%\ Q_{total}$ & $q_{\max} = 2.5^o C$ for stationary and moving analysis respectively. In figure 6b the upper horizontal axis, x_2, gives the ratio of the heat going into the tibial component to the total frictional heat; thus the graph can be used to calculate temperature rise for any partitioning of energy over the range $Q_t = 1\%\ Q_{total}$ to $Q_t = 50\%\ Q_{total}$.

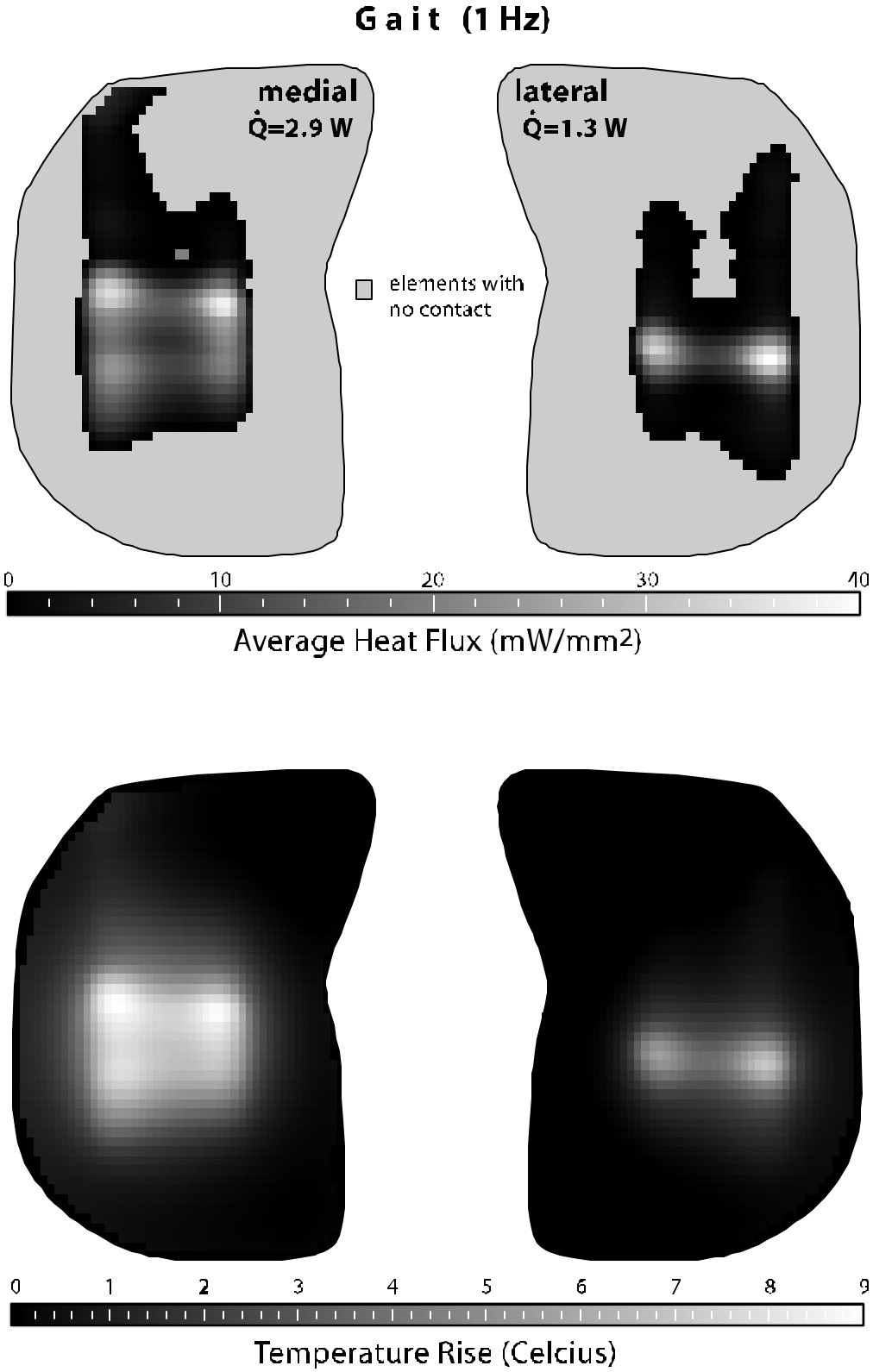

Figure 4-6: Contour maps for continuous stair activity for the 'standard condition' of a) the average frictional heat flux and b) the temperature rise in degrees Celsius. (1Hz, $k_f = 13$ W/(m·K), $m = 0.06$, $h = 30$ (W/(m^2·K))

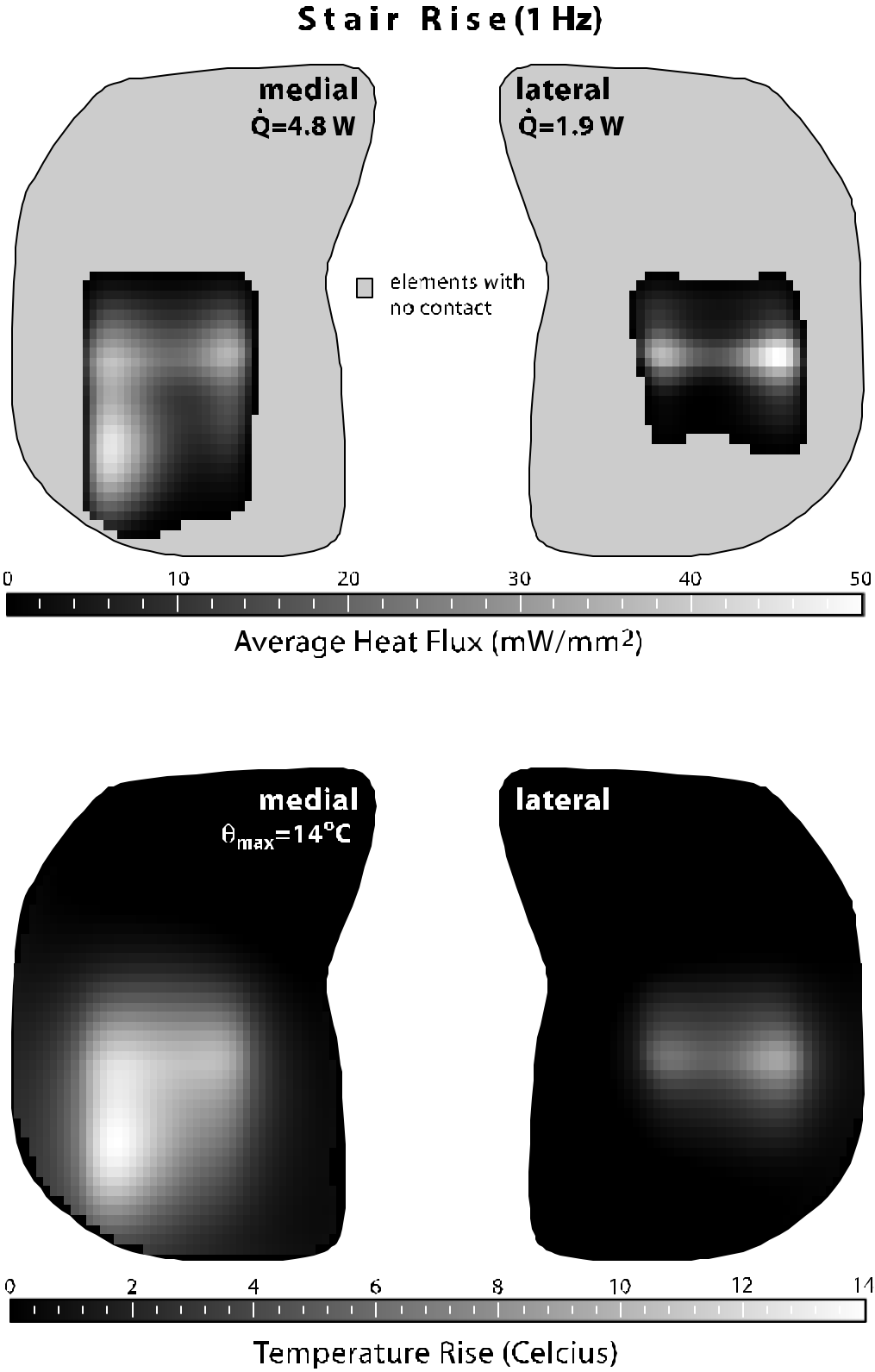

Figure 4-7: Contour maps for continuous stair activity for the 'standard condition' of a) the average frictional heat flux and b) the temperature rise in degrees Celsius. (1Hz, $k_f = 13$ W/(m·K), $m = 0.06$, $h = 30$ (W/(m^2·K))

Table 4-4: Conditions run off of the 'standard condition' (bold) and corresponding maximum temperature rise in degrees Celsius for the gait and stair activities accordingly.

	cycle frequency	femoral component thermal conductivity	convection heat transfer coefficient	maximum temperature rise	
				gait	stair
	(Hz)	k_f (W/m * K)	h (W/m^2 *K)	θ_{max} (K)	θ_{max} (K)
frequency excursions	0.50	13.00	30.0	4.5	7.2
	0.75	13.00	30.0	6.8	11.
	1.00	**13.00**	**30.0**	**9.1**	**14.**
	1.25	13.00	30.0	11.	18.
	1.50	13.00	30.0	14.	22.
	1.75	13.00	30.0	16.	25.
	2.00	13.00	30.0	18.	29.
thermal conductivity excursions	1.00	0.40	30.0	150.	240.
	1.00	1.30	30.0	71.	110.
	1.00	4.00	30.0	28.	44.
	1.00	**13.00**	**30.0**	**9.1**	**14.**
	1.00	40.00	30.0	3.0	4.8
convective heat transfer excursions	1.00	13.00	1.0	10.	16.
	1.00	13.00	3.0	10.	16.
	1.00	13.00	10.0	9.7	15.
	1.00	**13.00**	**30.0**	**9.1**	**14.**
	1.00	13.00	100.0	6.5	11.

The activity frequencies were varied between 0.5Hz and 2Hz. The nearly linear trend of frictional heating with activity frequency (Fig. 4-8 (a)) is expected. This can be most easily seen in Eqn 3.7, where the frictional heat flux is directly proportional to the sliding speed. The activity period is proportional to the kinematic path, which is essentially constant, divided by the speed. Activity frequency is the reciprocal of the

activity period; thus, activity frequency is directly proportional to speed. Similarly, though not shown, linear dependencies with friction coefficient were expected and found.

The very weak dependence on convection coefficient (Fig. 4-8 (c)) is somewhat surprising, but perhaps fortuitous. Because the frictional heat flux was discretized and time averaged for the various elements, the tibial surface has islands of frictional heating surrounded by regions of convective cooling. Any element that experiences contact is precluded from providing cooling. During these activities, elements are continuously exposed to both frictional heating and convective cooling. This mixture of heating and cooling would yield a lower average heat flux than that used by this solution procedure.

In vivo the knee does not go for thousands of cycles without a break. As discussed above this steady-state analysis takes average heat fluxes to predict the contact temperature. The time required for this system to reach steady-state was not explored. Thus, many interrupted activities may not reach the temperatures predicted here. The analysis is more similar to joint simulator machines that can run for hours or days without stopping.

The feasibility of these results are interesting given that many studies on the temperature rises for hip replacements find 1-10° C and the present results for the knee replacement are generally in line with those findings. Overall the analysis here aims to provide a simple first model for thermal analysis during continuous activities such as gait and stair for total knee replacements with UHMWPE tibial bearings. The findings from the standard conditions are most likely overestimates of actual steady-state temperature rises, primarily because of the heat partitioning and time averaging of the heat-flux,

which precludes frictional heating and convective cooling to operate on the same element.

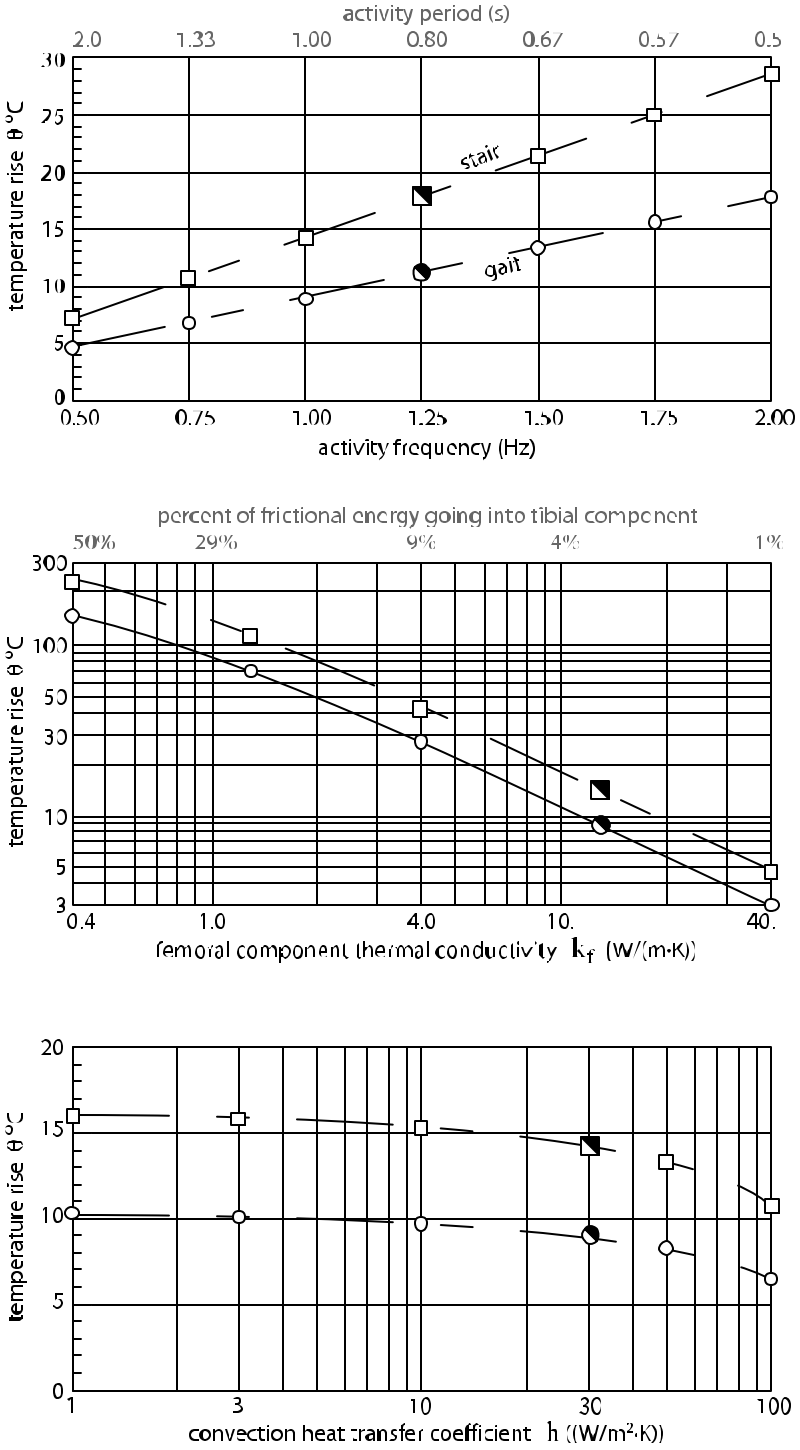

Figure 4-8: Plots of maximum temperature for variations in a) activity rate, b) thermal conductivity of the femoral component, and c) convection heat transfer coefficient.

CHAPTER 5

SUMMARY AND CLOSURE

Patients specific kinematic data derived from fluoroscopy has been a source of inputs for making wear predictions. Unfortunately, these measurements are based on 2-D x-ray images, and have uncertainties based on lack of depth perception and inaccuracies of the 3-D image matching. In the sagittal plane the errors can be as much as 0.5 mm, which is significant when wear depths are on the order of 1 mm. Fortunately, another group on campus has been working with multibody dynamics software and was able to import the data and optimize the motion of the two components based on elastic foundation. This group was capable of resolving unknowns which could not be determined through video fluoroscopy. The refined kinematics files were used with a custom software package for producing wear predictions, creep predictions, crossing motion analysis and thermal effects of gait and stair-rise exercises. The predictions were made using gait motion and stair-rise motion separately, but to predict damage for a retrieval a combination of the two motions was considered. Assuming the gait motion made up 70% of the patients total motion and the remainder was stair-rise motion, the area where damage occurred and the depth of the damage coincided with that found from the laser-scanned retrieval. Although this analysis has only been made for one implant and one patient, preliminary results are promising. Future work available for this project is refining the contact model used in the multibody dynamics software and implementing creep recovery models into the damage prediction software. Also validation of the thermal analysis could be performed using a motion which is easily reproduced experimentally.

APPENDIX A
CLASS HEIRARCHY FOR SOFTWARE DEVELOPED

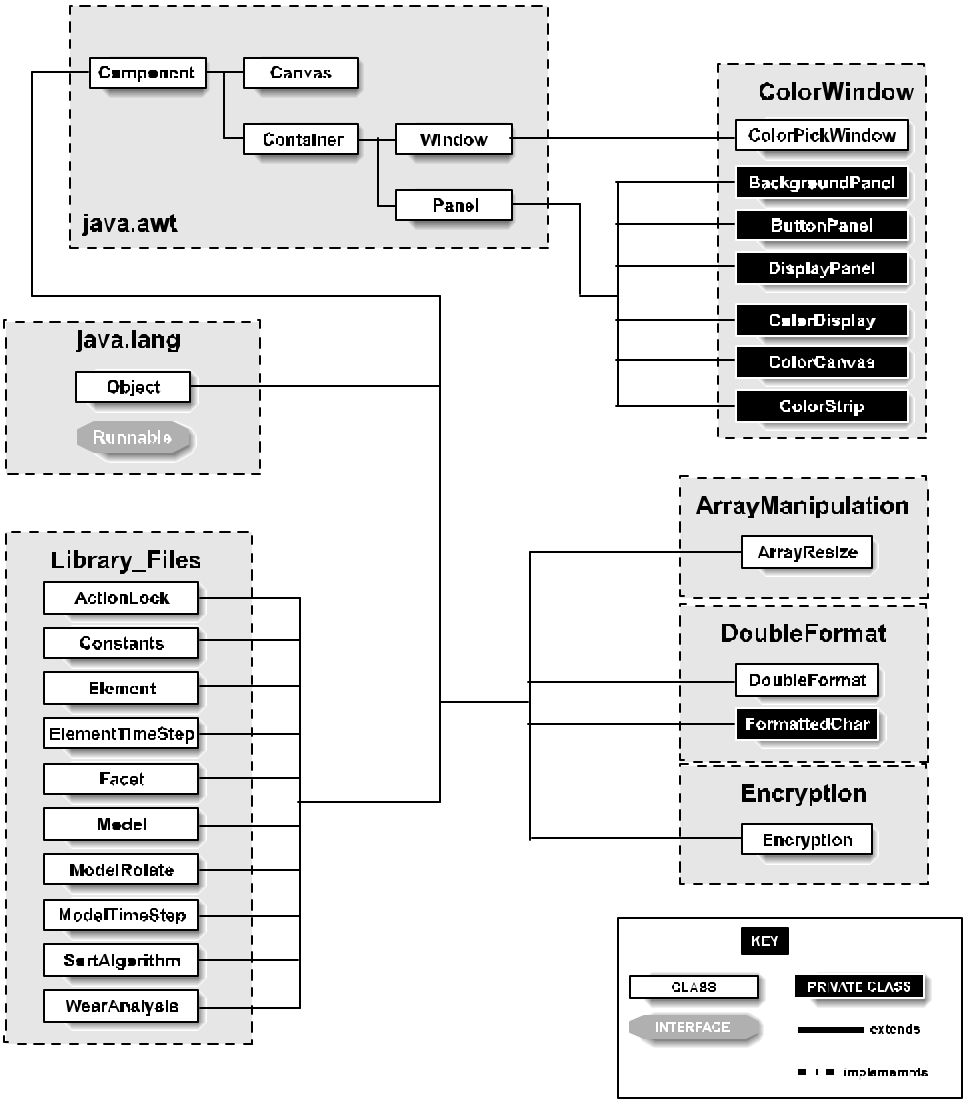

Figure A-1: Class hierarchy of java packages written for this project - Part 1. (ArrayManipulation, DoubleFormat, Encryption, ColorWindow, Library_Files).

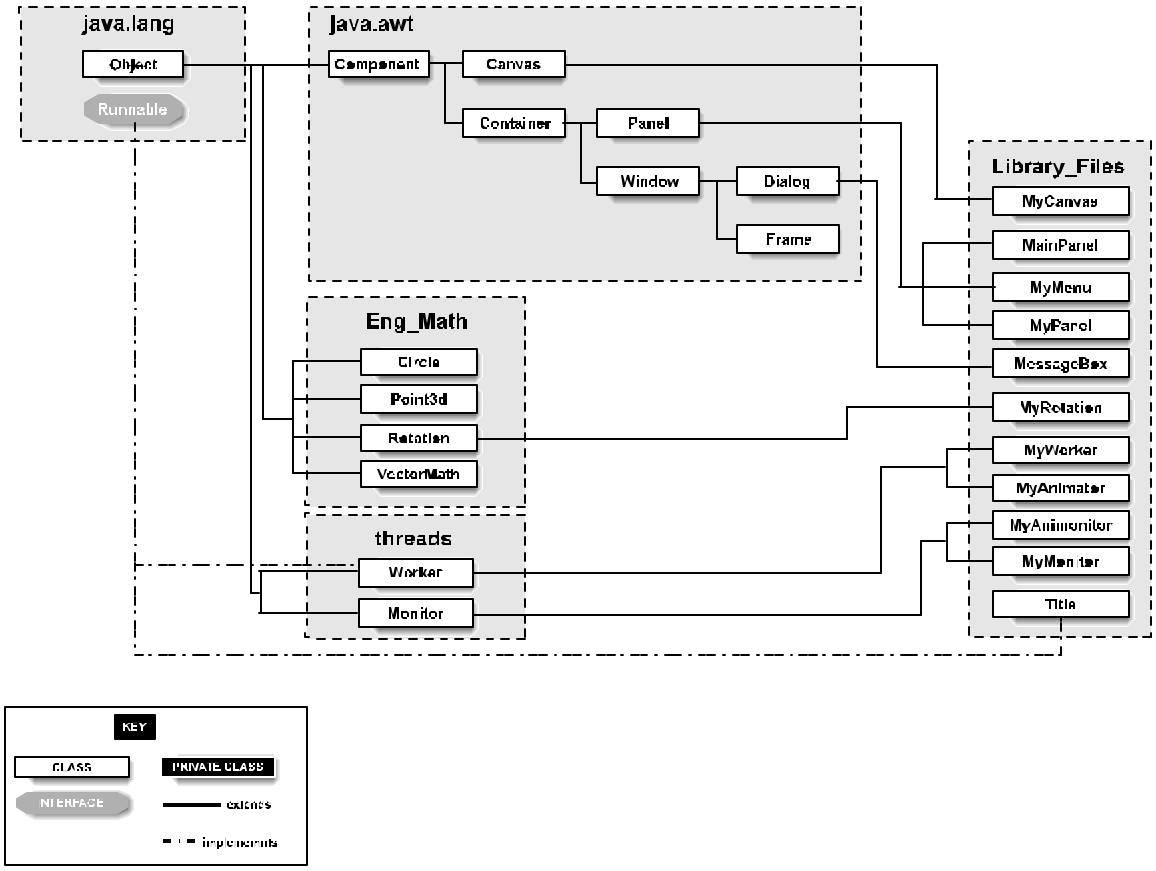

Figure A-2: Class hierarchy for java packages written for this project - Part 2. (Library_Files, Eng_Math, threads).

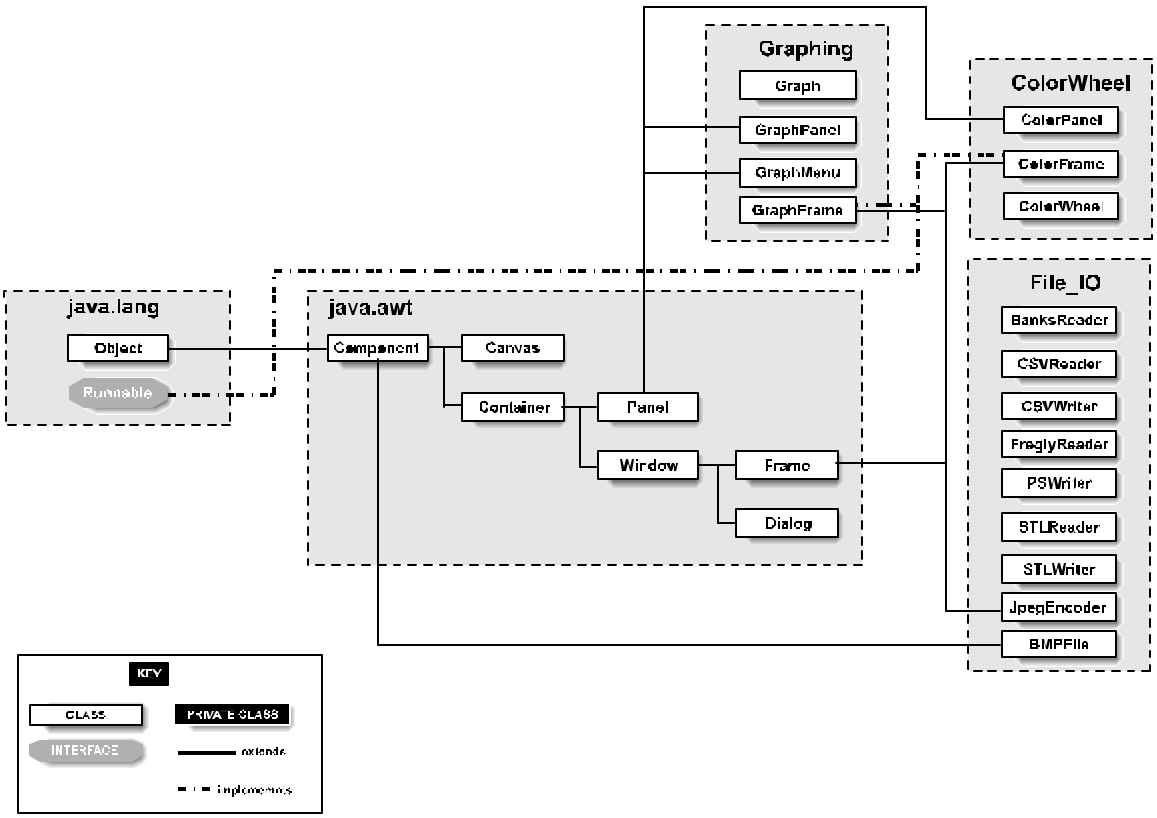

Figure A-3: Class hierarchy for java packages written for this project – Part 3. (Graphing, ColorWheel, File_IO).

APPENDIX B
DERIVATION OF ALGORITHMS

B.1 Temperature Rise Derivation

The temperature rise analysis begins with the differential heat conduction equation:

$$\frac{\partial^2 q}{\partial x^2}+\frac{\partial^2 q}{\partial y^2}+\frac{\partial^2 q}{\partial z^2}=\frac{1}{a}\frac{dq}{dt} \qquad \text{B-1}$$

This equation assumes a homogeneous solid, and is satisfied by the following:

$$q=\frac{Q}{8rC_p(pat)^{\frac{3}{2}}}e^{\frac{-\{(x-x')^2+(y-y')^2+(z-z')^2\}}{4at}} \qquad \text{B-2}$$

where Q is the heat released (J), r is the density $\left(\frac{kg}{m^3}\right)$, C_p is the specific heat $\left(\frac{J}{kg\cdot K}\right)$ and a is the thermal diffusivity $\left(\frac{m^2}{s}\right)$, and t is time (s). Knowing that

$$r^2=(x-x')^2+(y-y')^2+(z-z')^2 \qquad \text{B-3}$$

equation (2) simplifies to

$$q=\frac{Q}{8rC_p(pat)^{\frac{3}{2}}}e^{\frac{-r^2}{4at}} \qquad \text{B-4}$$

The above temperature rise is for a point source instantaneously releasing a packet of heat at a distance r from the point in question. The time that has passed since the heat was released is t. This solution can be integrated from the initial time corresponding to the first packet being released to the final time to give a temperature rise from a constant heat source at a constant distance producing a fixed flux for a known time period. The integral is described below:

$$q = \int_0^T \frac{\dot{Q}}{8 r C_p (p a t)^{\frac{3}{2}}} e^{\frac{-r^2}{4at}} dt \qquad \text{B-5}$$

where $\dot{q}$ is the energy released per unit time (W) and T is the total time the heat is released from the point source. By substituting $t = T - t'$ the solution for temperature rise becomes

$$q = \int_0^T \frac{\dot{Q}}{8 r C_p \left[p a (T - t')\right]^{\frac{3}{2}}} e^{\frac{-r^2}{4a(T-t')}} dt \qquad \text{B-6}$$

further substituting $t = (T - t')^{-1/2}$ the equation can be rewritten as

$$q = \int_{\frac{1}{\sqrt{T}}}^{\infty} \frac{\dot{Q}}{4 r C_p \left[p a\right]^{\frac{3}{2}}} e^{\frac{-r^2 t^2}{4a}} dt \qquad \text{B-7}$$

This equation can be evaluated and simplified to

$$q = \frac{\dot{Q}}{4p\,kr} erfc\left(\frac{r}{\sqrt{4at}}\right) \qquad \text{B-8}$$

where k is the thermal conductivity of the substance. If the equation is considered at very long times ($t \to \infty$), the temperature rise becomes only a function of material properties and distance from the heat source:

$$q = \frac{\dot{Q}}{4p\,kr} \qquad \text{B-9}$$

As mentioned earlier this solution is for a infinite solid or 'whole'-space, however, the solution required is for a 'half'-space indicating that the temperature rise would be doubled. Therefore,

$$q = \frac{\dot{Q}}{2p\,kr} \qquad \text{B-10}$$

This solution is considered for surface elements which are squares. Finding the solution for the maximum temperature rise on the surface requires integrating over the entire surface.

B.2 Crossing Motion Derivation

The starting point for determining the crossing intensity of a motion path is to define a vector whose direction will be used to measure all the directions against. This vector provides a reference for the other direction vectors. In this case, a vector from medial to lateral was chosen. Tribological intensity is a variable defined in this analysis as

$$\mathrm{T} = P \cdot d \qquad \text{B-11}$$

where P is the pressure at any point and d is the sliding distance over which the pressure is applied. In the software, each element has a time history of pressure, slip velocity and time increment. The equation for T can be rewritten as follows:

$$\mathrm{T}_i = P_i \left| V_i \right| \Delta t_i \qquad \text{B-12}$$

Tribological intensity for each timestep is calculated from the pressure (P) at the timestep, the magnitude of the slip velocity ($\left|V_i\right|$) at the timestep and the period of time which the two act (Δt_i).

An average direction of sliding is then calculated by using the angle created between the sliding vector and the arbitrary reference vector. The angle was measured, as shown in Figure 3-6, so that a unidirectional motion would yield a delta function. The angular measurement was weighted using tribological intensity as follows:

$$\bar{q} = \frac{\sum_{i=1}^{n} P_i \left|\overline{V_i}\right| \Delta t_i q_i}{\sum_{i=1}^{n} P_i \left|\overline{V_i}\right| \Delta t_i} \qquad \text{B-13}$$

The angle $\bar{q}$ represents the most probable sliding direction, or the direction receiving the most energy input. This value is used to determine how close to linearity the motion is by using a standard deviation calculation:

$$s = \sqrt{\frac{1}{n}\sum_{i=1}^{n}\left(P_i \left|\overline{V_i}\right| \Delta t_i \left(\bar{q} - q_i\right)\right)^2} \qquad \text{B-14}$$

This equation's result holds little value alone, but by normalizing it with respect to a motion which is varidirectional (a circular motion) whose tribological intensity is the same as the motion above the normalized value gives a result which is useful. The equivalent circular path can be described as follows:

$$s_o = \sqrt{\frac{1}{n}\sum_{i=1}^{n}\left(P_o \left|\overline{V_o}\right| \Delta t_o \left(\frac{p}{2} - q_o\right)\right)^2} \qquad \text{B-15}$$

$$P_o \left|\overline{V_o}\right| \Delta t_o = \frac{1}{n}\sum_{i=1}^{n}\left(P_i \left|\overline{V_i}\right| \Delta t_i\right) \qquad \text{B-16}$$

The normalized crossing motion intensity is defined as

$$s^* = \frac{s}{s_o} = \sqrt{\frac{\frac{1}{n}\sum_{i=1}^{n}\left(P_i \left|\overline{V_i}\right| \Delta t_i \left(\bar{q} - q_i\right)\right)^2}{\frac{1}{n}\sum_{i=1}^{n}\left(P_o \left|\overline{V_o}\right| \Delta t_o \left(\frac{p}{2} - q_o\right)\right)^2}} \qquad \text{B-17}$$

Various cases of motion and their corresponding crossing motion intensity are described in Figures 3-7, B-1 and B-2.

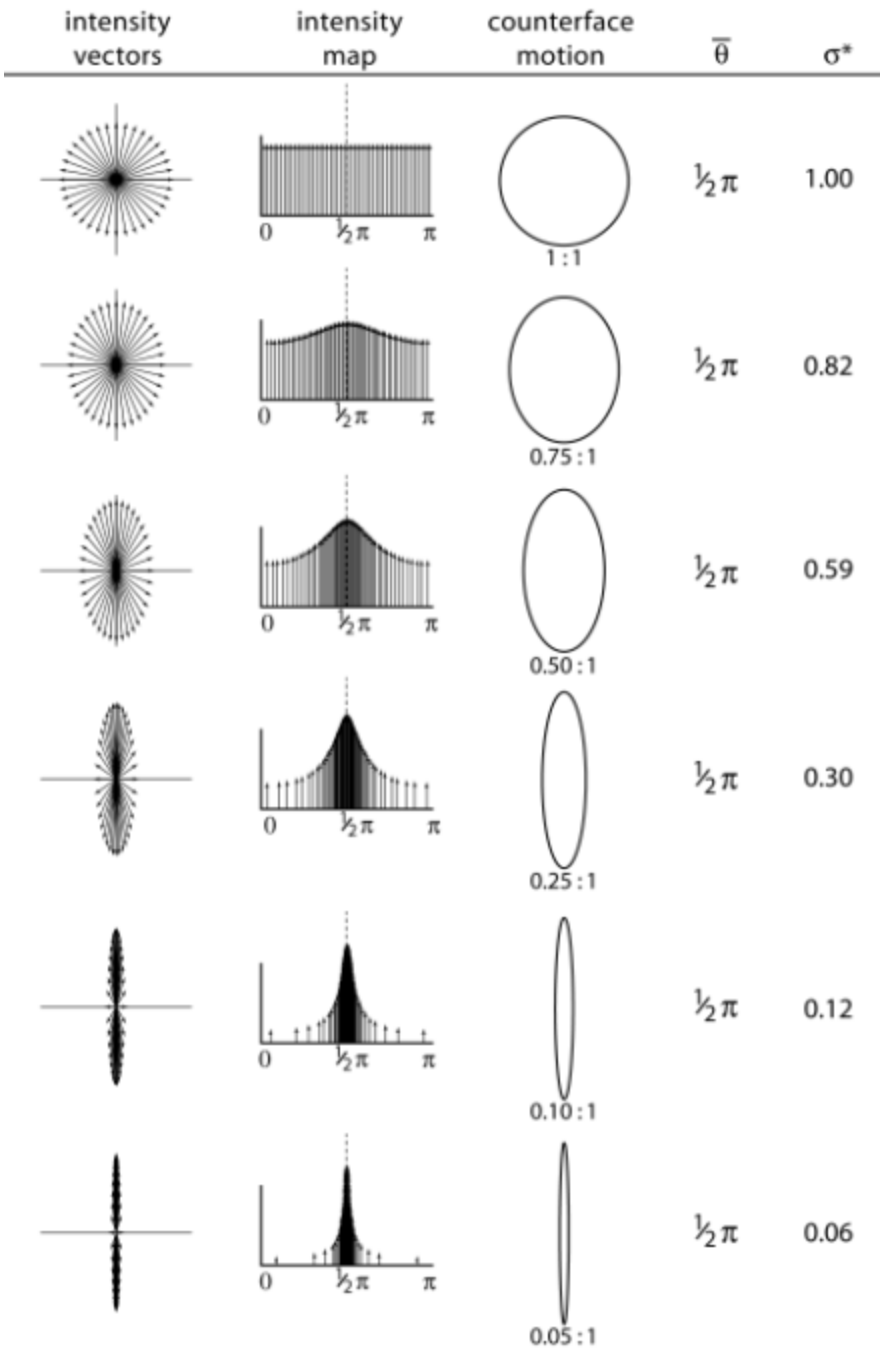

Figure B-1: Results of crossing intensity analysis with motion paths which are elliptical in nature.

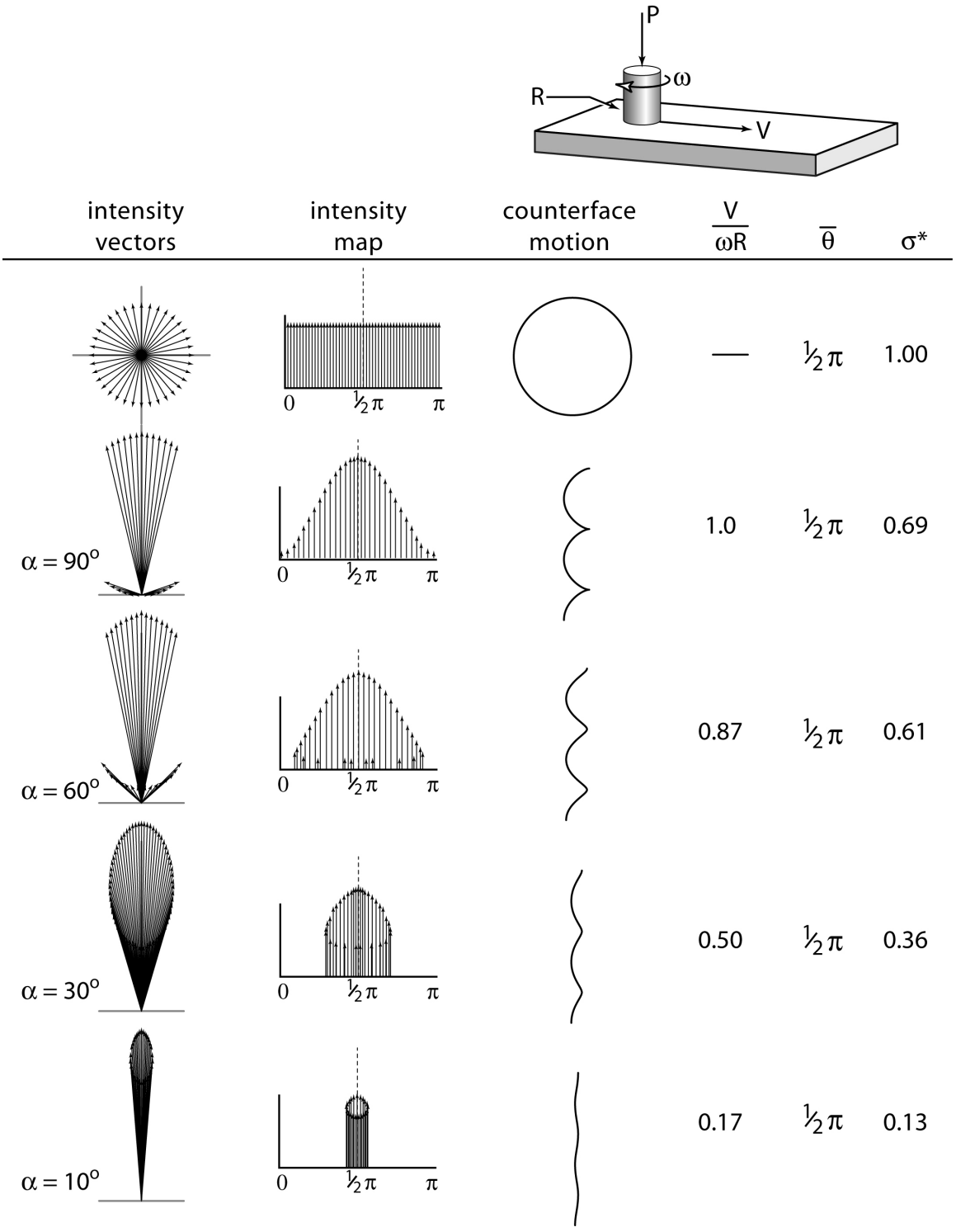

Figure B-2: Results of crossing intensity analysis with motion paths described by a pin rotating about its central axis while sliding linearly across a surface.

LIST OF REFERENCES

An, K.N., Himenso, S., Tsumura, H., Kawai, T., and Chao, E.Y.S. (1990). Pressure distribution on articular surfaces: application to joint stability analysis, *Journal of Biomechanics*, **23**, 1013-1020.

Archard, J.F. and Hirst, W. (1956). The wear of metals under unlubricated conditions, *Proceedings of the Royal Society*, **A236**, 397-410.

Asano, T., Akagi, M., Tanaka, K., Tamura, J., and Nakamura, T. (2001). In vivo three-dimensional knee kinematics using a biplanar image-matching technique, *Clinical Orthpaedics and Related Research*, **388**, 157-166.

Banks S.A. (1992). Model based 3D kinematic estimation from 2D perspective silhouettes: Application with total knee prostheses. PhD Dissertation, Massachusetts Institute of Technology, Cambridge, MA.

Banks, S.A., and Hodge, W.A. (1996). Accurate measurement of three-dimensional knee replacement kinematics using single-plane fluoroscopy, *Transactions on Biomedical Engineering*, **43**, 638-649.

Banks S.A., Markovich G.D., and Hodge W.A: (1997a). In vivo kinematics of cruciate-retaining and substituting knee arthroplasties, *Journal of Arthroplasty*, **12**, 297-304.

Banks S.A., Markovich G.D., and Hodge W.A. (1997b). The mechanics of knee replacements during gait: In vivo fluoroscopic analysis of two designs. *American Journal of Knee Surgery*, **10**, 261-267.

Bergmann, G., Graichen, F., Rohlmann, A., Verdonschot, N., and Van Lenthe, G. (2001a). Frictional heating of total hip implants. Part 1: Measurements in patients, *Journal of Biomechanics*, **34**, 421-428.

Bergmann, G., Graichen, F., Rohlmann, A., Verdonschot, N., and Van Lenthe, G. (2001b). Frictional heating of total hip implants. Part 2: Finite element study, *Journal of Biomechanics*, **34**, 429-435.

Beuchel, F., Beuchel, F., Pappas, M., and D'Alessio, J. (2001). Twenty-year evaluation of meniscal bearing and rotating platform knee replacement, *Clinical Orthopaedics and Related Research*, **388**, 41-50.

Bhushan, B. (1999). *Principles and Applications of Tribology*, John Wiley and Sons, New York.

Blankevoort, L., Kuiper, J.H., Huiskes, R., and Grootenboer, H.J. (1991). Articular contact in a three-dimensional model of the knee, *Journal of Biomechanics*, **24**, 1019-1031.

Bragdon, C.R., O'Conner, D.O., Lowenstein, J.D., Jasty, M., and Syniuta, W.D. (1996) The importance of multidirectional motion on the wear of polyethylene. *IMechE Part H: Journal of Engineering in Medicine* **210**, 157-165.

Burroughs, B.R., and Blanchet, T.A. (2001). Factors affecting the wear of irradiated UHMWPE, *Tribology Transactions*, **44**, 215-223.

Cadambi, A., Engh, G.A., Dwyer, K.A., and Vinh, T.N. (1994). Osteolysis of the distal femur after total knee arthroplasty, *Journal of Arthoplasty*, **9**, 579-594.

Carslaw, H.S., and Jaeger, J.C. (1959). *Conduction of Heat in Solids*, Oxford University Press, Oxford.

Chen, A., Mujtaba, M., Zucherman, J., Jeong, G., Joseph, T., Wright, K., and Di Cesare, P. (2001). Midterm clinical and radiographic results with the genesis I total knee prosthesis, *Journal of Arthroplasty*, **16**, 1055-1062.

Costigan, P., Deluzio, K., and Wyss, U. (2002). Knee and hip kinetics during normal stair climbing, *Gait and Posture*, **16**, 31-37.

Cripton, P.A. (1993). Compressive characterization of ultra-high molecular weight polyethylene with applications to contact stress analysis of total knee replacements, Master of Science Thesis. Queen's University, Kingston, Ontario.

Diduch, D., Insall, J., Scott, W., Scuderi, G., and Font-Rodriguez, D. (1997). Total knee replacement in young patients, *Journal of Bone and Joint Surgery*, **34**, 57-61.

Duffy, G., Trousdale, R., and Stuart, M. (1998). Total knee arthroplasty in patients 55 years or younger: 10-17 year results. *Clinical Orthopaedics and Related Research*, **356**, 22-27.

Fisher, J., Dowson, D., Hamdzah, H., and Lee, H.L. (1994). The effect of sliding velocity on the friction and wear of ultra-high molecular weight polyethylene for use in total artificial joints, *Wear*, **175**, 219-225.

Font-Rodriguez, D., Scuderi, G., and Insall, J. (1997). Survivorship of cemented total knee arthroplasty, *Clinical Orthopaedics and Related Research*, **345**, 79-86.

Godest, A.C., Beaugonin, M., Haug, E., Taylor, M., and Gregson, P.J. (2002). Simulation of a knee joint replacement during a gait cycle using explicit finite element analysis, *Journal of Biomechanics*, **35**, 267-273.

Godest, A.C., Simonis de Cloke, C., Taylor, M., Gregson, P.J., Keane A.J., Sathasivan, S., and Walker, P.S. (2000). A computational model for the prediction of total knee replacement kinematics in the sagittal plane, *Journal of Biomechanics*, **33**, 435-442.

Giddings, V.L., Kurtz, S.M., and Edidin, A.A. (2001). Total knee replacement polyethylene stresses during loading in a knee simulator, *Journal of Tribology*, **123**, 842-847.

Hahn, D.W., Wolfarth, and D.L., Parks, N.L. (1997). Analysis of polyethylene wear debris using micro-Raman spectroscopy: A report on the presence of beta-carotene, *Journal of Biomedical Materials Research*, **35**, 31-37.

Harman M.K., Banks S.A., and Hodge W.A: (2001). Polyethylene damage and knee kinematics after total knee arthroplasty, *Clinical Orthopaedics and Related Research*, **392**, 383-393.

Hoff, W., Komistek, R., Dennis, D., Gabriel, S., and Walker, S. (1998). Three-dimensional determination of femoral-tibial contact positions under in vivo conditions using fluoroscopy, *Clinical Biomechanics*, **13**, 455-472.

Howling, G.I., Barnett, P.I., Tipper, J.L., Stone, M.H., Fisher, J., and Ingham, E. (2001). Quantitative characterization of polyethylene debris isolated from periprosthetic tissue in early failure knee implants and early and late failure Charnley hip implants, *Journal of Biomedical Materials Research*, **58**, 415-420.

Hu, C., Liau, J., Lung, C., Huang, C., and Cheng, C. (2001). A two-dimensional finite element model for frictional heating analysis of total hip prosthesis, *Materials Science and Engineering*, **17**, 11-18.

Hurwitz, D.E., Sumer, D.R., Andriacchi, T.P., and Sugar, D.A. (1998). Dynamic knee loads during gait predict proximal tibial bone distribution, *Journal of Biomechanics*, **31**, 423-430.

Insall J.N., Dorr L.D., Scott R.D., and Scott, W.N. (1989). Rationale of the Knee Society clinical rating system, *Clinical Orthopaedics and Related Research*, **248,** 13-14.

Johnson, F., Scarrow, P., and Waugh, W. (1981). Assessments of loads in the knee joint. *Medical and Biological Engineering and Computing*, **19**, 237-243.

Johnson, K.L. (1985). *Contact Mechanics*, Cambridge University Press, Cambridge.

Kristensen, O., Nefei, A., Kjaersgaard-Andersen, P., Hvid, I., and Jensen, J. (1992). Long-term results of total condylar knee arthroplasty in rheumatoid arthritis, *Journal of Bone and Joint Surgery*, **74-B**, 803-806.

Laskin, R. (2001). The genesis total knee prosthesis, *Clinical Orthopaedics and Related Research*, **388**, 95-102.

Lee, K., and Pienkowski, D. (1998). Compressive creep characteristics of extruded ultra-high molecular weight polyethylene, *Journal of Biomedical Materials Research*, **39**, 261-265.

Li, G., Sakamoto, M., and Chao, E.Y.S. (1997). A comparison of different methods in predicting static pressure distribution in articulating joints, *Journal of Biomechanics*, **30**, 635-638.

Liao, Y.S., Lu, Z., Benya, P.D., and McKellop, H.A. (2002). Frictional heating and forced cooling of polyethylene-metal and polyethylene-ceramic bearing for hip joint replacement, In *Proceedings of the 48th Annual Meeting of the Orthopaedic Research Society*, February, Dallas, TX.

Lu, T.W., Taylor, S.J.G., O'Connor, J.J., and Walker, P.S. (1997). Influence of muscle activity on the forces in the femur: An in vivo study, *Journal of Biomechanics*, **30**, 1101-1106.

Kane, T.R. and Levinson, D.A. (1985). *Dynamics: Theory and Applications*. McGraw Hill, New York.

Komistek, R.D., Stiehl, J.B., Dennis, D.A., Paxson, R.D., and Soutas-Little, R.W. (1998). Mathematical model of the lower extremity joint reaction forces using Kane's method of dynamics, *Journal of Biomechanics*, **31**, 185-189.

Kurtz, S., Muratoglu, O., Evans, M., and Edidin, A. (1999). Advances in the processing, sterilization and crosslinking of ultra-high molecular weight polyethylene for total joint arthroplasty, *Biomaterials*, **20**, 1659-1688.

Kurtz, S., Villarraga, M., Herr, M., Bergstrom, J., Rimnac, C., Edidin, A. (2002). Thermomechanical behavior of virgin and highly crosslinked ultra-high molecular weight polyethylene used in total joint replacements, *Biomaterials*, **23**, 3681-3697.

Maxian, T.A., Brown, T.D., Pederson, D.R., and Callaghan, J.J. (1996). Adaptive finite element modeling of long-term polyethylene wear in total hip arthroplasty, *Journal of Bone and Joint Surgery*, **14**, 668-675.

Meding, J., Ritter, M., and Faris, P. (2001). Total knee arthroplasty with 4.4 mm of tibial polyethylene, *Clinical Orthopaedics and Related Research*, **388**, 112-117.

Meyer, D.M., and Tichy J.A. (1999). Lubrication model of an artificial hip joint: Pressure profile versus inclination angle of the acetabular cup, *ASME - Journal of Tribology*, **121**, 492-498.

Mikosz, R., Andriacchi, T., and Andersson, G. (1988). Model analysis of factors influencing the prediction of muscle forces at the knee. *Journal of Orhtopaedic Research,* **6**, 205-214.

Murataglu, O., Bragdon, C., O'Connor, D., Jasty, M., Harris, W., Rizwan, G., and McGarry, F. (1999). Unified wear model for highly crosslinked ultra-high molecular weight polyethylene, *Journal of Orthpaedic Research,* **13**, 143-146.

Nuño, N. and Ahmed, A.M. (2001). Sagittal profile of the femoral condyles and its application to femorotibial contact analysis, *Journal of Biomechanical Engineering*, **123**, 18-26.

Oonishi, H., Ishimaru, H., and Kato, A. (1996). Effect of cross-linkage by gamma radiation in heavy doses to low wear polyethylene in total hip prostheses, *Journal of Materials science: Materials in Medicine,* **7**, 753-763.

Pavone, V., Boettner, F., Fichert, S., and Sculco, T. (2001). Total condylar knee arthroplasty, *Clinical Orthopaedics and Related Research*, **388**, 18-25.

Premnath, V., Harris, W.H., Jasty, M., and Merrill, E.W. (1996). Gamma sterilization of UHMWPE articular implants: An analysis of the oxidation problem, *Biomaterials*, **17**, 1741-1753.

Ranawat, C.S., and Boachieadjei, O. (1988). Survivorship analysis and results of total condylar knee arthroplasty – 8-year to 11-year follow-up period, *Clinical Orthopaedics and Related Research*, **226**, 6-13.

Schipplein, O.D., and Andriacchi, T.P. (1991). Interaction between active and passive knee stabilizers during level walking, *Journal of Orthopaedic Research*, **9**, 113-119.

Schmalzried, T.P., and Callaghan, J.J. (1999). Wear in total hip and knee replacements, *Journal of Bone and Joint Surgery*, **81-A**, 115-136.

Schmalzried, T.P., Szuszczewicz, E.S., Northfield, M.R., Akizuki, K.H., Frankel, R.E., Belcher, G., and Amstutz, H.C. (1998). Quantitative assessment of walking activity after total hip or knee replacement, *Journal of Bone and Joint Surgery*, **80-A**, 54-59.

Scuderi, G.R., Insall, J.N., Windsor, R.E., and Moran, M.C. (1989). Survivorship of cemented knee replacements, *Journal of Bone and Joint Surgery-British Volume,* **71**, 798-803.

Seireg, A., and Arvikar, R. (1975). The prediction of muscular load sharing and joint forces in the lower extremities during walking, *Journal of Biomechanics*, **8**, 89-102.

Sextro, G., Berry, D., and Rand, J. (2001). Total knee arthroplasty using cruciate-retaining kinematic condylar prosthsis, *Clinical Orthopaedics and Related Research*, **388**, 33-40.

Taylor, S.J.G. and Walker, P.S. (2001). Force and moments telemetered from two distal femoral replacements during various activities, *Journal of Biomechanics*, **34**, 839-848.

Taylor, S.J.G., Walker, P.S., Perry, J.S., Cannon, S.R., and Woledge, R. (1998). The forces in the distal femur and the knee during walking and other activities measured by telemetry, *Journal of Arthroplasty,* **13**, 428-437.

Van Loon, C., Wisse, M., de Waal Malefijit, M., Jansen, R., and Veth, R. (2000). The kinematic total knee arthroplasty, *Archives of Orthopaedic Trauma and Surgery*, **120**, 48-52.

Waldman, S.D. and Bryant, J.T. (1997). Dynamic contact stress and rolling resistance model for total knee arthroplasties, *Journal of Biomechanical Engineering*, **119**, 254-260.

Wang, A., Essner, A., Polineni, V.K., Stark, C., and Dumbleton, J.H. (1998). Lubrication and wear of ultra-high molecular weight polyethylene in total joint replacements, *Tribology International*, **31**, 17-33.

Wang, A. (2001). A unified theory of wear of ultra-high molecular weight polyethylene in multidirectional sliding, *Wear*, **248**, 38-47.

Williams, J.I., Young, N., and Archinoff, R. (1994). Comparing a disease-specific measure and a functional status measurement in assessing the waiting-times and outcomes of hip and knee replacements, *Quality of Life Reasearch*, **3**, 99.

Wright, T.M., Rimnac, C.M., Stulberg, S.D., Mintz, L., Tsao, A.K., Klein, R.W., and McCrae, C. (1992). Wear of polyethylene in total joint replacements, *Clinical Orthopaedics and Related Research*, **276**, 126-134.

Young, T.H., Cheng, C.K., Lee, Y.M., Chen, L.Y., and Huang, C.H. (1999). Analysis of ultrahigh molecular weight polyethylene failure in artificial knee joints: Thermal effect on long-term performance, *Journal of Biomedical Materials Research*, **48**, 159-164.

BIOGRAPHICAL SKETCH

The author was born in Orlando, Florida, in 1978. Throughout his life he excelled at mathematics and sciences. In high school he earned the Bright Futures scholarship, which helped him to pay for school at the University of Florida. The author majored in mechanical engineering with a minor in computer science as an undergraduate, and received the Society of Tribologists and Lubrication Engineers scholarship award. After graduating in 2001, he decided to continue his work by going to graduate school at the University of Florida.